Journal of Building Technology, 2024, Volume 6, Issue 2
DOI: 10.32629/jbt.v6i2.2584
ISSN Online: 2717-5103
ISSN Print: 2705-1390

Assessment of a Force Method for the Resilient Seismic Design of Special Moment-Resisting Steel Frames with Hysteretic Energy Dissipation Devices

Héctor Hernández Ramírez[1], Arturo Tena Colunga[2]

1. Postgraduate in Structural Engineering, Universidad Autónoma Metropolitana Azcapotzalco, Av. San Pablo 180, Col. Reynosa Tamaulipas, 02200 Mexico City, Mexico.
2. Materials Department, Universidad Autónoma Metropolitana Azcapotzalco, Av. San Pablo 180, Col. Reynosa Tamaulipas, 02200 Mexico City, Mexico.

Abstract: In this paper, the authors present the results of nonlinear dynamic analyses of twelve building models designed according to a methodology based upon the force method, capacity design principles and the concept of structural fuses to achieve resilient seismic designs for special moment-resisting steel frames with hysteretic energy dissipation devices mounted on chevron steel bracing. It is demonstrated that the resilient design mechanism previously checked with pushover analyses is also attained for most studied models with nonlinear dynamic analyses using an acceleration record which is compatible with the elastic design spectrum. Also, it is corroborated that the planned second line of inelastic defense is activated if the seismic action surpasses the considered design spectrum. Based upon the obtained results, it is confirmed that it is possible to perform a resilient seismic design for the studied system under the proposed methodology, even for tall and slender buildings. Therefore, the proposed initial stiffness ratio parameters and the global design parameters previously proposed by the authors to use in a code-oriented force method can be used with confidence for the resilient seismic design of this structural system.

Key words: resilient seismic design; hysteretic energy dissipation devices; structural fuses; ductile steel moment frames

1. Introduction

Seismic response control in Mexico has developed since the damage caused by the earthquake of September 19, 1985 in Mexico City (Del Valle, 1988). In the last thirty years, the number of experimental and analytical studies on energy dissipation devices proposed and tested worldwide has grown considerably (Tena-Colunga, 2007).

In fact, for more than two decades, there have been publications related to the design of structures with hysteretic energy dissipaters, either by validating design methods based on the concept of additional equivalent viscous damping (Wu and Hanson 1987, Scholl 1993, Foti et al. 1998, Ramirez et al. 2001, Benedetti et al. 2014) or by means of displacement design procedures (e.g. Ramirez et al. 2001, Chen et al. 2007, Symans et al. 2008).

However, there is only very little research available that has been oriented to promote designs in compliance with current regulations, either for structural repair proposals (Tena-Colunga and Pérez-Moreno 1994, Tena-Colunga et al. 1996,

Tena-Colunga and Vergara 1997, Tena 1998a, Aguiar et al. 2016a), or by defining global seismic design parameters (Vargas and Bruneau 2006 and 2009, Tena and Nangullasmú 2013, Tena-Colunga and Nangullasmú-Hernández 2015, Nangullasmú and Tena 2016, Tena et al. 2016, Tena and Hernández 2016, Tena-Colunga and Hernández-Ramírez 2017, Tena and Gama 2017) that allow designing new structures with DOE using the force method according to the guidelines of current seismic design regulations (Tena and Nangullasmú 2013, Tena-Colunga and Nangullasmú-Hernández 2015, Nangullasmú and Tena 2016, Aguiar et al. 2016b, Tena et al. 2016, Tena and Hernández 2016, Tena-Colunga and Hernández-Ramírez 2017, Tena and Gama 2017).

In the previously cited works, the general seismic design methodology proposed by this research team to define global seismic design parameters for frame-based structures with hysteretic energy dissipaters mounted on chevron type windbreaks as structural fuses has been succinctly presented. This methodology can be transparently inserted into future versions of the Mexican seismic design regulations and recommendations. The step-by-step seismic design process has also been exemplified with the design of a 15-story ductile structural steel building with chevron counterbuckling mounted DDEs as structural fuses, and its subsequent detailed evaluation through nonlinear static and dynamic analyses (Hernandez 2015, Tena and Hernandez 2017). This paper presents the validation of the robustness of the proposed resilient and capacity design procedure by comparing the response from stepwise nonlinear dynamic analyses with respect to the nonlinear static analyses under increasing monotonic load (pushover). The resilient design mechanism and the global seismic design parameters were defined and reported in more detail in Hernández (2015), Tena and Hernández (2016), and Tena-Colunga and Hernández-Ramírez (2017).

2. General Information About the Study

As described in more detail in previous works (Hernández 2015, Tena and Hernández 2016 and 2017, Tena-Colunga and Hernández-Ramírez 2017), 270 ductile structural steel frames with chevron-type steel counterwinds supporting the hysteretic dissipaters were designed and studied (Figure 1), based on the following hypotheses that favor a resilient seismic design:

A. The flat frames are competent to resist the vertical loads and their proportion of the design seismic forces, but responding in the range of elastic behavior;

B. The counter-framing system, which supports the energy dissipaters, behaves elastically, and;

C. The hysteretic dissipaters are the only ones that should ideally work inelastically under the action of an intense earthquake.

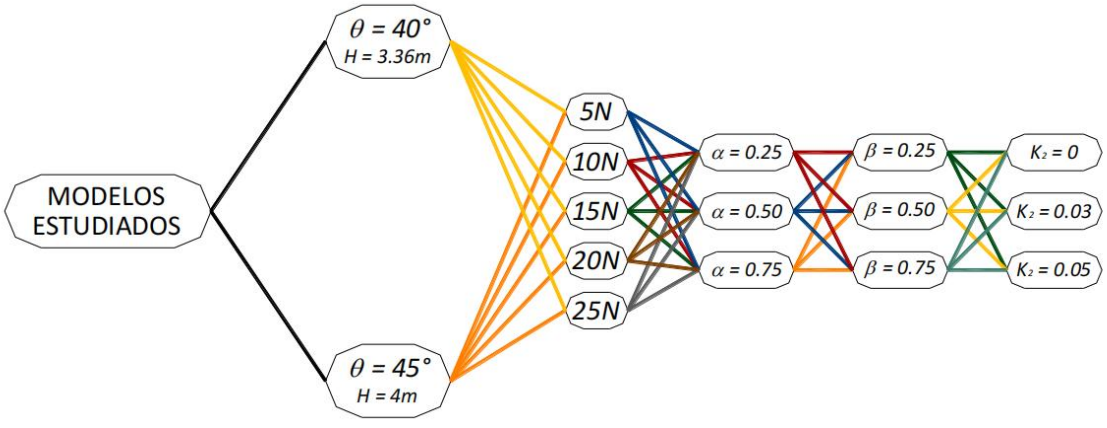

Figure 1. Schematic tree diagram of the models studied by Hernández (2015).

Steel frames were considered that are part of office building, located in Mexico City, whose details are described in previous works (Hernandez 2015, Tena and Hernandez 2016, Tena-Colunga and Hernandez-Ramirez 2017). Five different building heights were considered, ranging from five to 25 levels (Figure 1), with intermediate increments of five levels (Figures 1 and 2). For the analysis of the models, two angles of inclination in the windbreaks are defined, θ=40° and 45°, which have mezzanine heights of 3.36 m and 4 m, respectively, as illustrated in the elevations of Figure 3.

It was proposed that the changes in the cross-sections of the frame elements should not coincide with those of the wind-spreader system, in order to avoid the formation of weak floors, due to the contrasts in stiffness and resistance, as schematically illustrated in Figure 2.

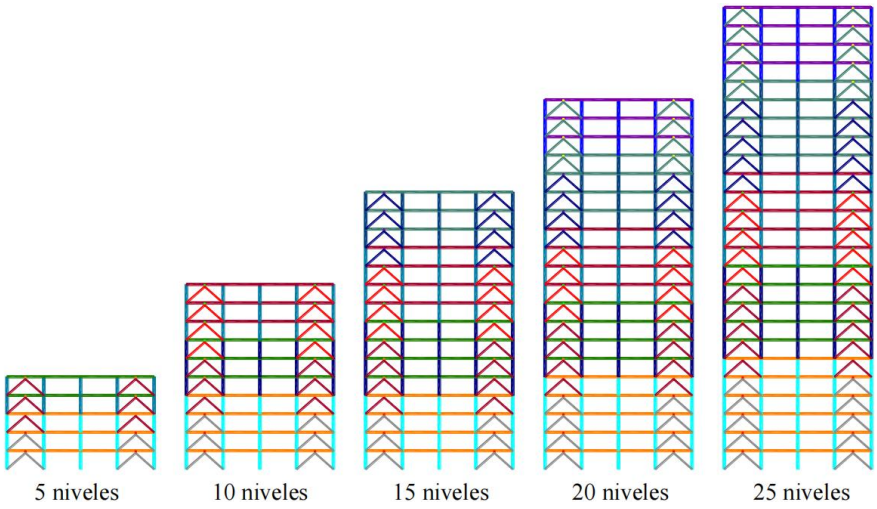

Figure 2. Representation of cross-section changes for the structural steel frames studied. The colors schematically illustrate the section changes, but have no relation between one model and another (i.e., they do not indicate that they are the same cross-section).

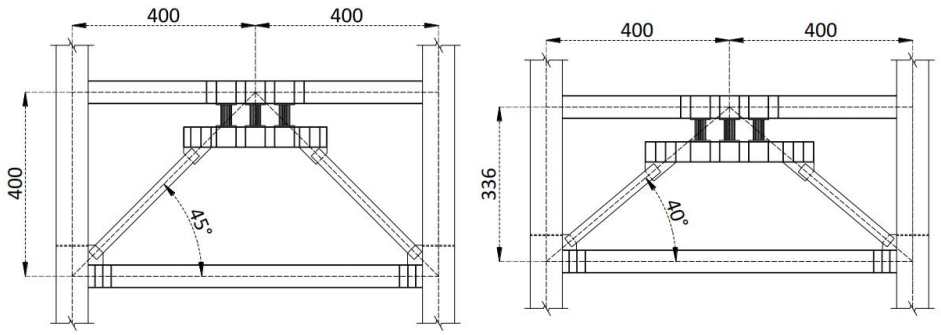

Figure 3. Configuration of counter-ventilated bays (dimensions in centimeters)

2.2 Structural parameters

As described in greater detail in previous works (Hernández 2015, Tena and Hernández 2016, Tena-Colunga and Hernández-Ramírez 2017), structural parameters were studied with the purpose of defining values that allow, as far as possible and practical, a resilient seismic design, where the structural steel frames remain essentially elastic or with a very low inelasticity and the energy dissipaters concentrate the inelastic deformation, since they can be replaced in a faster and cleaner way, if there is, of course, sufficient budget for it.

The variables studied were (Figure 1):

a) The ratio of the lateral stiffness provided by the frames (K frame) to the total lateral stiffness of the dissipative frame-windshield system (K total):

$$\alpha = \frac{K_{frame}}{K_{total}} \qquad (1)$$

b) The ratio of the lateral elastic stiffness of the energy dissipater (K_{DDE}) to the lateral stiffness of the supporting wind girders (K_{diag}):

$$\beta = \frac{K_{DDE}}{K_{diag}} \qquad (2)$$

c) The variation in the post-creep slope developed by the hysteretic energy dissipators, normalized with respect to the initial elastic slope, identified by the variable K_2 (Figure 4).

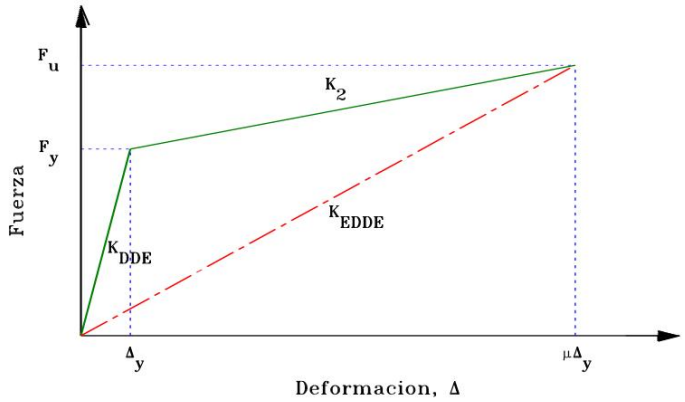

Figure 4. Typical force-deformation curve of a hysteretic heatsink with bilinear behavior.

3. Definition of Ultimate Resilient Seismic Mechanisms

The 270 models under study were designed using a procedure based on the initial elastic stiffness of frames with dissipators presented in more detail in Hernandez (2015), Tena and Hernandez (2016, 2017). In order to have a defined comparison reference, an effective seismic design shear of 10% the total weight of the structure (V/W_t=0.10) was considered for all models, which corresponds to the effective basal design shear of a ductile structure (Q=4 and R=2) of the most demanded lake area of Mexico City as established in NTCS-04 (2004). Also, the target local ductility of the hysteretic dissipators was assumed μ_d=10.

The proposed design procedure involves an iterative process, in addition to incorporating concepts of design by capacity. In this approach, the design is performed sequentially from the weakest element (where the energy will be dissipated) to the strongest (which should remain elastic). Therefore, it is intended to promote a resilient seismic design philosophy, where the energy dissipaters serve as structural fuses against lateral loads and, consequently, are the only elements that should be replaced after an intense earthquake.

3.1 Definition of a resilient mechanism

The standard used to define the final acceptable mechanism is that it should be resilient, which is in sharp contrast to the collapse prevention mechanism standards advocated by many seismic design regulations around the world, which basically consider it acceptable for structures to be severely damaged and almost unusable after a design earthquake, or to be unusable for months or years while developing and implementing effective restructuring strategies to extend their service life. Therefore, the ultimate acceptable mechanism was defined by ensuring that, upon reaching the target ductility of the energy dissipaters (μd), the other structural elements remained essentially elastic, especially the supporting wind bracing and columns. At most, the incipient creep of the beams was accepted as a second adequate source of inelasticity that could cope with extreme actions beyond those considered in their design.

3.2 Color scale to identify inelastic demands

To verify the general resilient design assumptions stated above, it was necessary to monitor the potential inelastic response of all structural elements, not just the energy dissipaters. Therefore, in addition to defining the bilinear curves of the energy dissipaters, the theoretical plastic rotation capacity of the beams and columns and the potential buckling of the wind bracing were also modeled. For the steel elements, their plastic interaction and moment-curvature diagrams were calculated from the classical theory of plasticity for steel sections and box sections, as detailed in Hernandez (2015) for the particular case of the box section.

As 270 different models were designed and analyzed in the parametric study (Figure 1), in order to analyze and discriminate which combinations of global design parameters met the objective of obtaining the resilient mechanism described above, a warm color scale was defined to identify in a simple and schematic way the level of inelastic demand of the different structural elements. The warm color scale for the energy dissipaters was set according to the ductility demands developed by the models, and are identified in Figure 5a. For congruence, a scale was also defined for the wind girders (Figure 5b), in the hope that it would not be required, as in fact happened in the 270 cases under study. For structural steel I-section beams, the curve behaves symmetrically for both positive and negative bending (Figure 5c, $P/P_y=0$). For box-section columns, the effect of axial force on the nominal bending resistance of the columns is considered, i.e., for the relationship of $P/P_y > 0$, the plastic moment will decrease (Figure 5c).

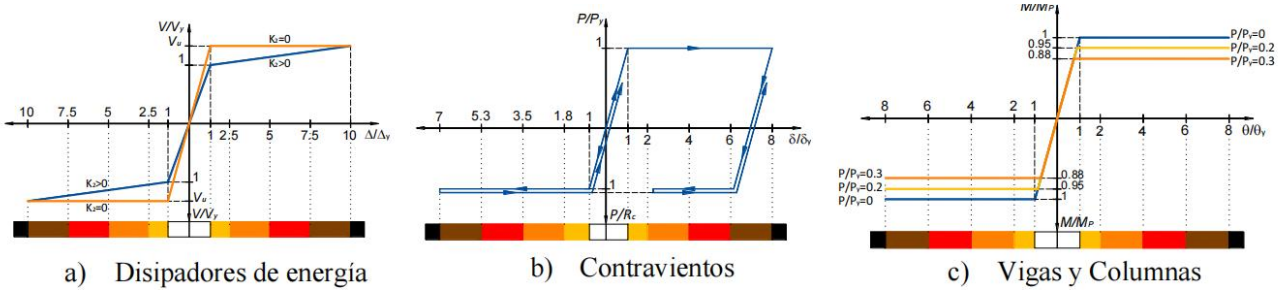

a) Disipadores de energía b) Contravientos c) Vigas y Columnas

Figure 5. Warm color scale to identify inelastic demands.

Heatsinks with perfect elastoplastic behavior ($K_2=0$) or with effective post-creep slopes ($K_2>0$) were designed from the outset to provide the same ultimate strength V_u at the target ductility μ_d. It can be seen from Figure 5a that the heatsink creep shear (V_y) is lower for heatsinks with post-creep slopes $K_2>0$ than for perfect elastoplastic behavior ($K_2=0$), and therefore heatsinks with $K_2\neq0$ start working earlier in the range of inelastic behavior than perfect elastoplastic heatsinks.

3.3 Stiffness balances

Based on the detailed analysis of the inelastic fluences mappings and ductility demands of the dissipaters, structural stiffness parameter balances α and β were defined for the studied models, leading to a resilient seismic design, according to the concept that hysteresis energy dissipaters work as structural fuses.

Tables 1 and 2 present the ranges of combinations of parameters α and β for which the use of structures with energy dissipaters is recommended when the angle of inclination of the wind bracing with respect to the horizontal plane is θ=40° or θ=45° respectively. For this case, it was decided to use the following color coding in the tables to relate the parameters α, β and Q to the following behavior observed in the creep mappings of the frame elements: (a) without color when the frame behaves elastically or there are less than five ends of structural elements with incipient creep, (b) with light yellow when there are more than five ends of beams with incipient creep, but not more than 15, (c) with yellow when there are more than 15 ends of beams with incipient creep, but less than 30, d) with orange when there are more than 30 beam ends with creep and, e) with carmine red when the magnitude of the creep at the ends of the beams is moderate or large, regardless of

the number of beams. It should be noted that the color of the parameter α is related when fluences are observed in the beams and is indicated with the maximum intensity indicated by β for their combinations with K_2/K_{DDE}, for space-saving purposes when preparing and synthesizing this information. Therefore, if in a group of information, there are β cells shaded in yellow and orange, for that group the α value for which those behaviors are obtained is identified in orange.

Table 1. Range of recommended values for structural parameters when θ=40°, ductile structural steel frames

Levels	α	K_2/K_{DDE}	Q		
			β=0.25	β=0.5	β=0.75
5	0.25 - 0.75	0	5.8	4.5 - 4.3	4.2 - 3.7
		0.03	5.4 - 6.4	4.9	4.5 - 4.2
		0.05	5.6 - 6.4	5.0 - 5.2	4.7 - 4.4
10	0.25 - 0.75	0	3.9 - 3.7	3.7	3.4
		0.03	4.4 - 4.0	4.1 - 4.3	3.7 - 3.9
		0.05	4.6 - 4.3	4.3 - 4.6	3.9 - 4.1
15	0.25 - 0.75	0	3.2 - 3.0	3.1 - 3.0	2.9 - 3.1
		0.03	3.6 - 3.1	3.4 - 3.5	3.3 - 3.6
		0.05	3.8 - 3.4	3.6 - 3.9	3.5 - 3.9
20	0.25 - 0.75	0	2.9 - 2.7	2.8 - 2.6	2.7 - 2.6
		0.03	3.2 - 2.8	3.1 - 2..8	3.0 - 2.9
		0.05	3.4 - 2.8	3.3 - 3.1	3.2
25	0.25 - 0.75	0	2.8 - 2.6	2.6 - 2.5	2.5 - 2.6
		0.03	2.9 - 2.8	2.7 - 2.8	2.7 - 2.8
		0.05	3.0 - 2.8	2.9 - 2.9	2.9

Table 2. Range of recommended values for structural parameters when θ=45°, structural steel ductile frames

Levels	α	K_2/K_{DDE}	Q		
			β=0.25	β=0.5	β=0.75
5	0.25 - 0.75	0	4.7 - 5.2	4.0 - 4.1	3.8 - 3.5
		0.03	5.1 - 5.6	4.5 - 4.7	4.2 - 4.0
		0.05	5.3 - 5.7	4.7 - 5.0	4.4 - 4.2
10	0.25 - 0.75	0	3.5 - 3.5	3.3 - 3.1	3.2 - 3.1
		0.03	4.0 - 3.6	3.7 - 3.1	3.6
		0.05	4.3 - 3.6	4.0 - 3.9	3.8 - 3.9
15	0.25 - 0.75	0	2.9 - 2.9	2.8 - 2.6	2.7 - 2.6
		0.03	3.3 - 3.0	3.1 - 2.9	2.9 - 3.1
		0.05	3.5 - 3.1	3.3 - 3.0	3.1 - 3.4
20	0.25 - 0.75	0	2.6 - 2.7	2.5 - 2.4	2.6 - 2.3
		0.03	3.0 - 2.6	2.9 - 2.5	2.8 - 2.5
		0.05	3.2 - 2.7	3.0 - 2.6	2.9 - 2.7
25	0.25 - 0.75	0	2.9 - 2.7	2.7 - 2.5	2.6 - 2.4
		0.03	3.0 - 2.7	2.6 - 2.6	2.5 - 2.5
		0.05	3.0 - 2.6	2.6 - 2.5	2.5 - 2.7

From the results shown in Table 1, it can be concluded that, for the design basal shear considered (V/W_t=0.10), the design of ductile steel frames with hysteresis energy dissipative devices mounted on chevron wind bracing with tilt angles θ=40° operating with the structural fuse concept (elastic frame, inelastic dissipaters) is highly probable for almost all heights (5 to 25 levels) and parameter combinations under study: $0.25\leq\alpha\leq0.75$, $0.25\leq\beta\leq0.75$ and $0.0\leq K_2/K_{DDE}\leq0.05$. The exceptions where some incipient fluences are present in beams (yellow color) are for the following combinations: a) α=0.75 and β=0.25 with K_2/K_{DDE}=0.0 and K_2/K_{DDE}=0.03 for the 15-level models and, b) α=0.75, β=0.25 and K_2/K_{DDE}=0.03 for the 20- and 25-level models. Only moderate beam fluences (orange color) are obtained when α=0.75, β=0.25 and K_2/K_{DDE}=0.0 for the 20- and 25-level models.

In contrast, it can be concluded from the analysis of the results shown in Table 2 that the range of combinations of the parameters α, β and K_2/K_{DDE} for which ductile structural steel frames with hysteretic energy dissipaters mounted on chevron windscreens can be designed under the structural fuse concept is markedly reduced when the angle of the windscreen is increased to $\theta=45^0$. It was only possible for all five-level models, and also for the 10-level models, except when α=0.75 and β=0.25, particularly for perfect elastoplastic behavior (K_2/K_{DDE}=0.0), where a code orange is obtained. From the 15-level models onwards, a significant number of beam fluences start to be observed when α=0.75 and β=0.25, and grow for the 20-level models, where significant beam fluences are appreciated when: a) α=0.75 and β=0.25 and, b) α=0.75 and β=0.50. For the 25-level models, creep in beams is unavoidable for all combinations of α and β under study, but tends to decrease as both β and K_2/K_{DDE} increase.

Therefore, from the analysis of the results shown in Tables 1 and 2, it can be concluded that for the effective design basal shear V/W_t=0.10 considered, as the models grow in number of stories (they become slimmer), the fluences in the frame beams begin to appear because: (a) the elastic stiffness of the dissipator decreases with respect to that of the supporting wind girders (parameter β decreases), (b) the elastic lateral stiffness of the frame grows with respect to that of the wind girder-dissipator system (parameter α increases) and, (c) the effective post-creep slope (K_2/K_{DDE}) decreases, particularly for perfect elastoplastic behavior (K_2=0). Similarly, the inelastic action in the frame elements (beams in this case) increases as the angle of inclination of the crosswinds with respect to the horizontal plane (θ) increases, even though a very small increase of θ (only five degrees) was considered in this study. The above had already been derived analytically in previous studies (Tena 2000), when deriving the nonlinear equation for single-span frames with energy dissipating devices mounted on chevron wind girders, considering that the wind girder remains elastic and the dissipator has a bilinear behavior and can develop a given ductility.

3.4 Global seismic design parameters according to Mexican seismic design guidelines.

The determination of global seismic design parameters, such as the seismic performance factor Q, the reduction factor for over-resistance R, the interstory distortion at creep (Δ_y) and the ultimate design distortion (Δ_u) compatible with a resilient seismic design where the energy dissipaters work as structural fuses at the maximum possible ductility, ensuring that the structure responsible for vertical loads remains essentially elastic, is presented and discussed in detail in Hernández (2015), Tena and Hernández (2016) and Tena-Colunga and Hernández-Ramírez (2017). Some relevant aspects yielded from that detailed study are summarized below.

The estimated values for the global ductility of the system (seismic behavior factor Q) were obtained for all models and stiffness balances α and β considered in this study, and are synthetically reported in Tables 1 and 2. From these tables, it is observed that the Q factor decreases as: a) the number of stories increases, b) β increases, c) K_2/K_{DDE} decreases and, d) α decreases. However, it should be noted that the impact of α appears to be less than for the other parameters in this structural system.

According to the seismic design regulations and manuals in force in Mexico until the end of 2017, the maximum value allowed for the seismic behavior factor Q is Q=4. It can be seen in Tables 1 and 2 that close and higher values can be obtained for the five and 10 level models (if $K_2 \neq 0$), but these are reduced for heights greater than 15 levels and for 25 levels reach a value close to Q=3.0, if the system is maintained with the concept of a resilient design where the energy dissipaters work as structural fuses. Of course, larger values can be obtained if severe creep is allowed in the frame beams, but what would be the purpose of losing the advantages of a resilient design where an elastic response of the frame is ensured and, therefore, the operation of the building is guaranteed after the occurrence of an intense earthquake, with minimum interruptions that can be programmed to replace the energy dissipaters if required?

The obtained over-resistance factors varied in the following intervals: a) $1.8 \leq R \leq 2.7$ when $\alpha=0.25$, b) $2.3 \leq R \leq 3.3$ when $\alpha=0.50$ and, c) $2.9 \leq R \leq 4.4$ when $\alpha=0.75$. The parameter with the greatest influence on the over-resistance factor is the stiffness balance between the frame and the overall system, α, since as α increases, the frame takes a greater proportion of the lateral load and, given the sequence in a design by capacity, the beams and columns are over-designed with respect to the energy dissipating devices. The second most influential parameter is the post-creep slope K_2; in fact, larger over-resistance factors are obtained as K_2 decreases. The impact of the parameter β on the over-resistance is less clear, generally as the value of β increases the over-resistance tends to decrease or stay with the same value, for most cases. As the value of the wind angle θ is increased, the over-resistance decreases in general. It is again confirmed that the over-resistance depends both on the system and on the structural configuration, something that should be recognized, or at least commented, in all seismic design regulations in Mexico.

It was found that the creep interstory distortions (Δy) for this structural system vary between 0.08% and 0.43%, and the following general trends of Δy with the parameters under study (Hernandez 2015, Tena and Hernandez 2016): a) as α increases, Δ_y increases, b) as β increases, Δ_y decreases, and c) as the number of floors increases, Δ_y tends to increase. In addition, it is also observed from the results obtained that the distortions Δ_y for $\theta=45°$ were larger than those corresponding to $\theta=40°$, so, apparently, as θ increases, Δ_y increases.

The average ultimate interstory distortions were obtained by calculating the average for each ratio of α and β. Only the interstories where the energy dissipaters (and, in some cases, certain beams) had inelastic deformations were used. That is, the interstories that remained elastic were not taken into account for the calculation of the average distortions. In the parametric study, it was appreciated that, in general, the ultimate distortions increase with height and with the angle of inclination of the windage, θ (Hernández 2015, Tena and Hernández 2016). The ultimate distortions developed at the target ductility of the heatsinks $\mu_d \approx 10$ under resilient design were less than 1.3%, which clearly indicates that in a well-designed ductile steel frame with energy dissipaters mounted on chevron counterwinds, very high interstory distortions need not be developed to dissipate a large amount of energy and develop reasonable overall ductilities. Since the maximum ultimate distortions are moderate, it is clear that employing hysteretic energy dissipaters designed with resilient and structural fuse concepts are also a reasonable option to minimize damage to displacement-sensitive contents and to nonstructural elements that are properly decoupled from the main structural system.

4. Evaluation of the Resilient Mechanism by Nonlinear Analysis

The results of the extensive parametric study described above, mainly all the results obtained from the nonlinear static analyses in the face of monotonic-increasing (pushover) loading, are reported in detail in Hernández (2015) and in other previously published works (Tena and Hernández 2016, Tena-Colunga and Hernández-Ramírez 2017).

4.1 Selected models

In this work, in order to illustrate that the design procedure is adequate and reasonable under the action of intense earthquakes, including those in which the actions exceed those considered in the elastic seismic design spectra, the results of the nonlinear static analyses under increasing monotonic load ("pushover") and nonlinear stepwise dynamic analyses of twelve of the 270 models are compared, which for ease of interpretation are identified in Table 3.

Table 3. Models studied to compare the results of nonlinear static and dynamic analyses

Model	Levels	θ	α	β	k_2/k_{DDE}	T (s)
m5α75β25	5	450	0.75	0.25	0.05	0.762
m10α25β 25	10	450	0.25	0.25	0.00	1.240
m10α75β25-1	10	450	0.75	0.25	0.00	1.302
m10α75β25-2	10	450	0.75	0.25	0.03	1.343
m10α 75β25-3	10	450	0.75	0.25	0.05	1.372
m15α 75β25-1	15	450	0.75	0.25	0.05	1.842
m15α 75β25-2	15	400	0.75	0.25	0.05	1.547
m15α 50β50	15	400	0.50	0.50	0.03	1.550
m20α 50β75-1	20	450	0.50	0.75	0.05	2.162
m20α 50β75-2	20	400	0.50	0.75	0.05	1.773
m25α75β25	25	450	0.75	0.25	0.05	2.295
m25α75β75	25	400	0.75	0.75	0.03	1.851

When selecting a model, sampling was attempted for different heights and parameter combinations. Based on the results of the pushover analysis, the design method obtained the most tests. As in many cases, it can be seen from these results that some beams may experience creep. This can be inferred by comparing the summaries in Tables 1 and 2 with the model shown in Table 3.

Therefore, considering that theoretically all five-level models have the potential to achieve a 100% elastic design mechanism (Tables 1 and 2), it was decided to test the theoretically most unfavorable combination of stiffness parameters that promote the inelasticity of the frame beam, using the maximum α parameter (α=0.75), the smaller β parameter (β=0.25) with the angle θ of 45^0. The 10-level models were selected for comparison because, as synthetically indicated in Table 2, inelastic beam influences are expected (α=0.75), and they were compared with models where a fully resilient response is expected (α=0.25). For the 15-level models, we wanted to compare the difference in the response of the wind uplift inclination angle when, according to the pushover analyses, it was obtained that for α=0.75 and β=0.25, for $\theta=45^0$ fluences in beams should be expected before the design action when $k_2/k_{DDE}=0.05$ (Table 2), while for that same combination of parameters, a resilient behavior is expected for $\theta=40^0$ (Table 1). The behavior should also be resilient for 15 levels and when $\theta=40^0$ and α=β=0.50 (Table 1). For the 20-level models, acceptable combinations were evaluated, although not 100% resilient, considering values of α=0.50 and β=0.75 that according to pushover analyses, may lead some beam fluences to the target ductility of the dissipators for $\theta=45^0$ (Table 2), but to a more satisfactory behavior when $\theta=40^0$ (Table 1). For the 25-level models, a critical scenario was evaluated where many beam fluences are accepted for both $\theta=45^0$ (when $k_2/k_{DDE}=0.05$, Table 2) and $\theta=40^0$ (when $k_2/k_{DDE}=0.03$, Table 1). Using these critical case studies, the robustness of the method and the parameters proposed previously (Hernández 2015, Tena and Hernández 2016 and 2017, Tena-Colunga and Hernández-Ramírez 2017) is reasonably evaluated, because, if there are no important differences even for the cases where 100% resilient behavior is not expected (only the dissipators work inelastically), they are also not present in theoretically more favorable cases.

4.2 Acceleration record selected for the nonlinear dynamic analyses

To perform the nonlinear dynamic analyses, a synthetic acceleration record generated by Perez Rocha for station CO56 of the accelerometric network of the Valley of Mexico (S56-EW) was selected, associated with a subduction earthquake similar to that of September 19, 1985 (Ms=8.1) and representative of the soft ground zone of Mexico City (Roma Norte). The dominant period of the site is Ts=2.2s. The synthetic acceleration record and its corresponding response spectra for two viscous dampings (ξ=2% and ξ=5%), are presented in Figure 6, as well as the elastic design spectrum (Q=1) according to Appendix A of NTCS-04 (2004).

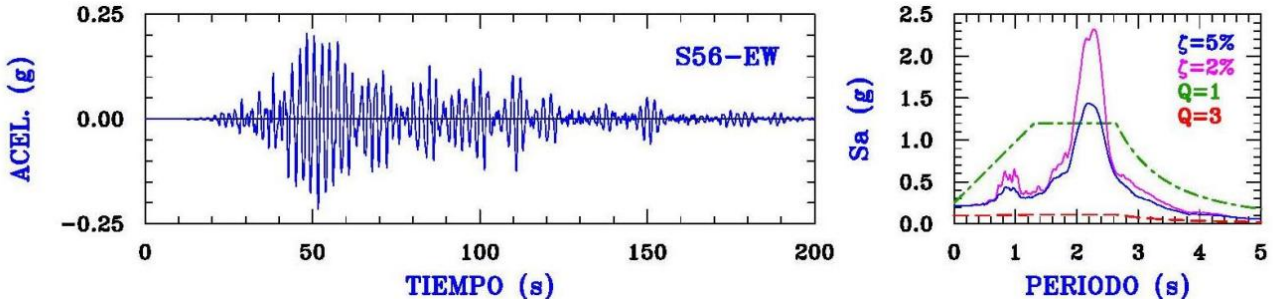

Figure 6. Artificial acceleration record for station 56 (S56-EW) for an earthquake similar to that of September 19, 1985 (Ms=8.1) and acceleration spectra for ξ=2% and ξ=5%, as well as elastic (Q=1) and inelastic (Q=3 and R=2.5) design spectra for site CO56.

When the equivalent viscous damping is 5% (ξ=5%), the selected record shows a maximum false acceleration (c=1.2g) that is 25% higher than the elastic design spectrum (Q=1) calculated according to Appendix A of NTCS-04; When the equivalent viscous damping is 2% (ξ=2%), it is 93% higher.

Therefore, it is a severe accelerogram that aims to evaluate the reserves of the system under the action of an earthquake that exceeds the actions considered in the design, something that unfortunately already happened in Mexico City on September 19, 1985, where the pseudoacceleration response spectrum at the SCT site exceeded four times the maximum ordinate of the design spectrum of the 1976 Federal District Regulation, as discussed in Rosenblueth et al. (1989) and graphically illustrated in Tena (2010).

For reference, we also present what would be a design spectrum according to Appendix A of the NTCS-04, if Q=3 and R=2.5 were used, which are global average design parameters (e.g., Tables 1 and 2) and practical parameters that could be proposed for design according to that standard for the models under study. Thus, from this spectrum identified with Q=3, it is obtained that the design pseudo-acceleration in the interval of fundamental elastic vibration periods in which the models are found ($0.762s \leq T \leq 2.295s$) is $c=S_a=0.11g$, 10% higher than the value nominally considered in the design of all models ($c=V/W_t=0.10$). In other words, the models under study would be underdesigned by 10% with respect to the regulatory spectrum if it is also considered that the equivalent viscous damping is 5% (ξ=5%).

The nonlinear dynamic analyses were performed considering both 5% and 2% viscous damping for the following reasons. It is a very common design practice to employ the elastic spectrum for ξ=5% and not to correct that spectrum for lower damping, as should be the case in steel structures with welded connections. Under these conditions, the results of the analyses for 5% viscous damping would be more representative of the general assumption made in the design of the models and, therefore, their comparison should be closer to that obtained with the pushover analyses. However, since considering ξ=2% would be more realistic (although conservative) of the initial viscous damping of steel structures with welded connections, it is also interesting to evaluate what would be the maximum responses and the pattern of creep that could occur when the design forces are underestimated under an extreme action, in this case, both for the action and for overestimating the damping that is more representative for that type of structures.

4.3 Analysis of 5, 10, 15, 20, 25-level models

4.3.1 5-level model

Figure 7 presents the comparative inelastic fluences mappings obtained for the m5α75β25 model (Table 3), both from the pushover analysis for the target ductility of the energy dissipaters (μ_d), and from the nonlinear dynamic analyses for ξ=5% and ξ=2%. In this case, it can be seen that there is a significant coincidence in the spatial location and relative magnitude of the flowing dissipators between the pushover analysis and the nonlinear dynamic analyses, although it should be noted that the intensities of the dissipator fluences are lower in the nonlinear dynamic analyses than those obtained with the pushover analysis, as a consequence that, for this model, given its elastic fundamental period (Table 3), the onset is reasonably far from resonant responses (Figure 6).

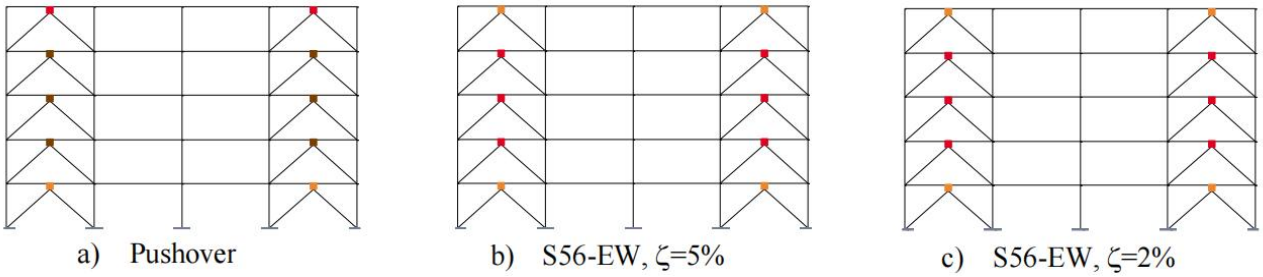

Figure 7. Comparative inelastic fluences mappings for the m5α75β25 model (θ=45^0, k_2/k_{DDE}=0.05).

This observation is confirmed by the results presented in Figure 8, where the maximum ductility demands of the energy dissipators, maximum interstory distortions, and maximum interstory shears are reported. Indeed, it is observed that the curves obtained from the pushover analysis adequately cover those obtained from the nonlinear dynamic analyses, where, as expected, higher demands are obtained when ξ=2% is considered than when ξ=5% is considered. Additionally, it is observed that the energy dissipators develop ductility demands higher than six even when interstory distortions are lower than 1%. It is verified that the ultimate mechanism obtained before the extreme dynamic design action for the considered site is 100% resilient.

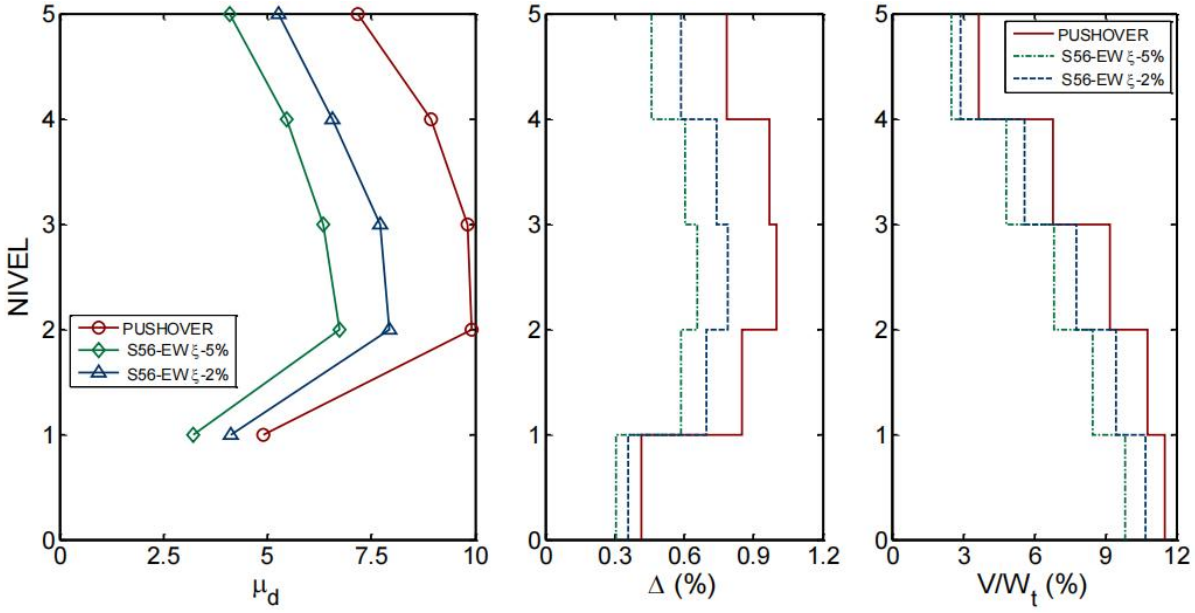

Figure 8. Comparative ductility demands μ_d of energy dissipaters, maximum interstory distortions and maximum shear forces in interstories, for model m5α75β25 (θ=45^0, k_2/k_{DDE}=0.05).

The results obtained also allow one to illustrate and comment on aspects that are very important and that should be taken into account in the seismic-resistant design of structures in general, since they are not only present in structures with energy dissipaters: (a) the convenience that the elastic fundamental period of the designed structure is far away from the site period (T_s), to avoid undesirable resonant responses, (b) when high values of ductility reduction (Q) are considered in the seismic design, notwithstanding that the fundamental period of the structure is far away from the site period, inelastic responses of importance will be irremediably presented in the structure before the action considered for the site (in this case, in terms of the ductility of the dissipaters). For the model under study, the design obtained turned out to be 100% resilient and also favored, because the structure has a fundamental period of vibration reasonably far from the resonant fringe, which an expert designer really interested in protecting people and their heritage should always look for, within the general constraints of the design project entrusted to him.

4.3.2 10-level models

Figure 9 presents the comparative inelastic fluences mappings obtained for the m10α25β25 model (Table 3). According to the results of the pushover analysis, the ultimate mechanism expected under the design seismic action should be 100% resilient, with exclusive fluences in the dissipators (Figure 9a). The creep mappings obtained from the nonlinear dynamic analyses agree reasonably well with those from the pushover analysis for both ξ=5% (Figure 9b) and ξ=2% (Figure 9c). Again, it should be noted that the intensities of the heatsink fluences are lower in the nonlinear dynamic analyses than those obtained with the pushover analysis, as a consequence, for this model, given its elastic fundamental period (T=1.24s, Table 3), it is reasonably far from resonant responses, although already in the frankly rising branch of the spectrum (Figure 6).

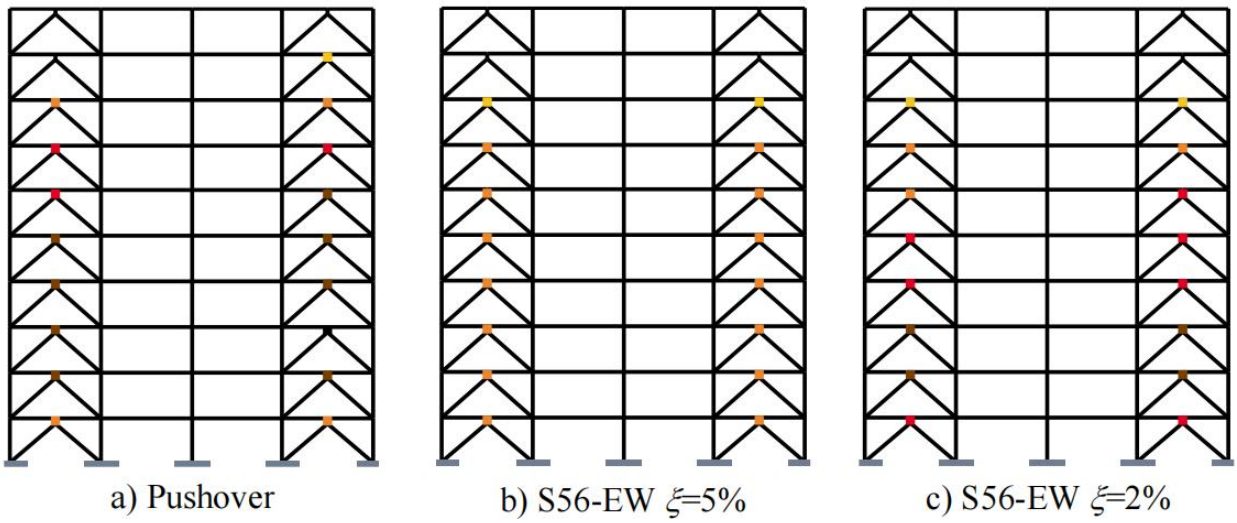

Figure 9. Comparison of the inelastic fluences mappings for the m10α25β25 model ($\theta=45^0$, $k_2/k_{DDE}=0$).

This observation is again confirmed by the results of the maximum ductility demands of the energy dissipaters, the maximum interstory distortions and the maximum interstory shears presented in Figure 10, where it is verified that the curves obtained from the pushover analysis cover satisfactorily well those obtained from the nonlinear dynamic analyses for ξ=5% and even for ξ=2%, with the exception of the maximum demands for the first level. Again, the energy dissipaters develop high ductility demands for interstory distortions less than 1%. The mechanism obtained under extreme dynamic action is again 100% resilient.

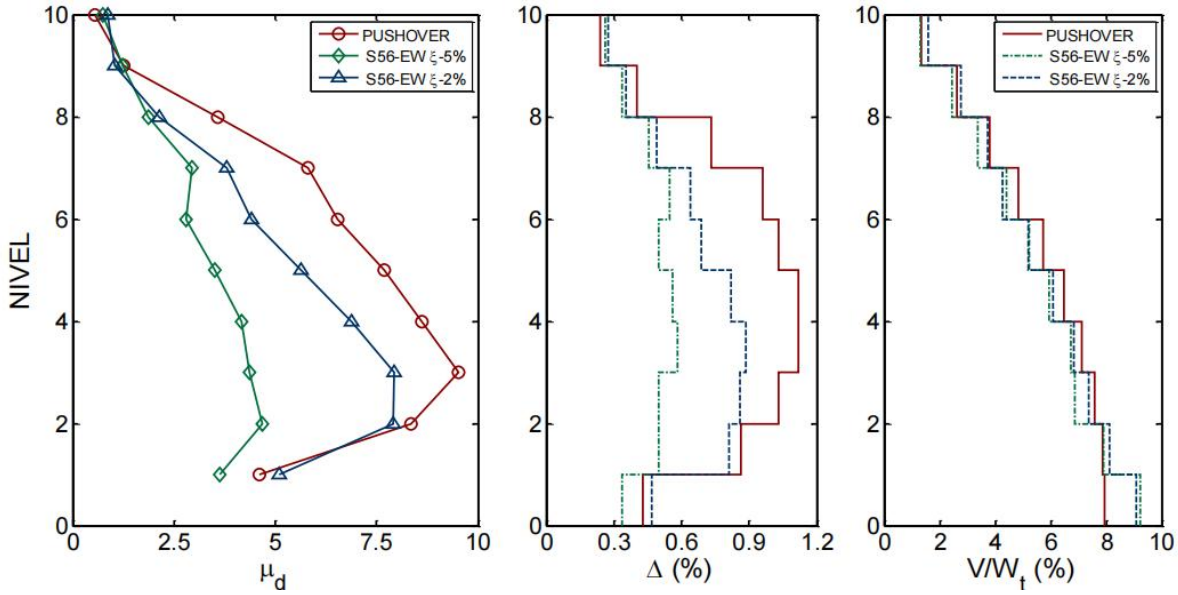

Figure 10. Comparative ductility demands μ_d of the energy dissipaters, maximum interstory distortions and maximum shear forces in the interstories, for model m10α25β25 ($\theta=45^0$, $k_2/k_{DDE}=0$).

Figures 11 to 16 present the results for three models that were designed with the same stiffness balances, $\alpha=0.75$ and $\beta=0.25$, but where the cross-sections of the frame resisting elements vary somewhat as a result of assuming different post-creep slopes of the dissipators, $k_2/k_{DDE}=0$ (perfect elastoplastic, Figures 11 and 12), $k_2/k_{DDE}=0.03$ (Figures 13 and 14) and $k_2/k_{DDE}=0.05$ (Figures 15 and 16), which is also reflected in the fundamental periods of vibration reported in Table 3. According to the pushover analyses of each model, if taken to the target ductility $\mu_d=10$ of the critical dissipators, incipient creep is expected in some beams, occurring relatively more for the perfect elastic-plastic case (Figure 11a), than when designed for post-creep slopes of 3% (Figure 13a) and 5% (Figure 15a).

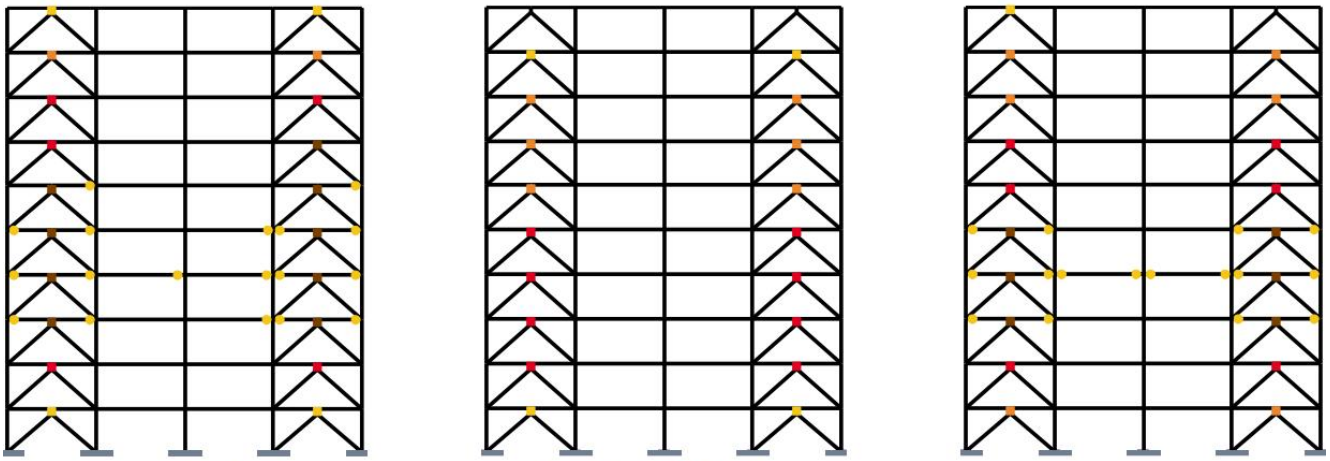

Figure 11. Comparison of inelastic fluences mappings for the m10α75β25-1 model ($\theta=45^0$, $k_2/k_{DDE}=0$).

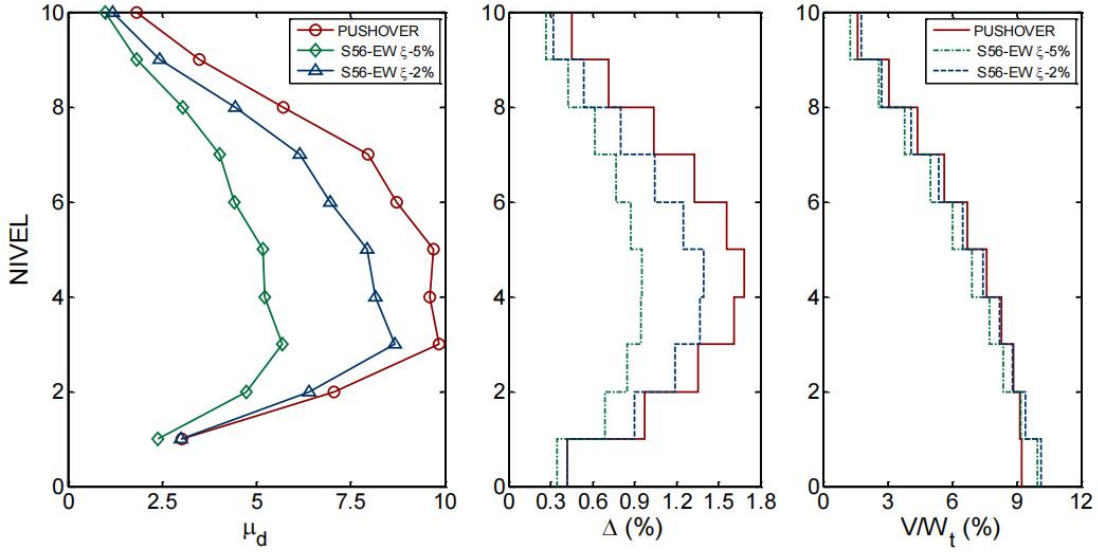

Figure 12. Comparative ductility demands μ_d of the energy dissipaters, maximum interstory distortions and maximum shear forces in the interstories, for model m10α75β25-1 ($\theta=45^0$, $k_2/k_{DDE}=0$).

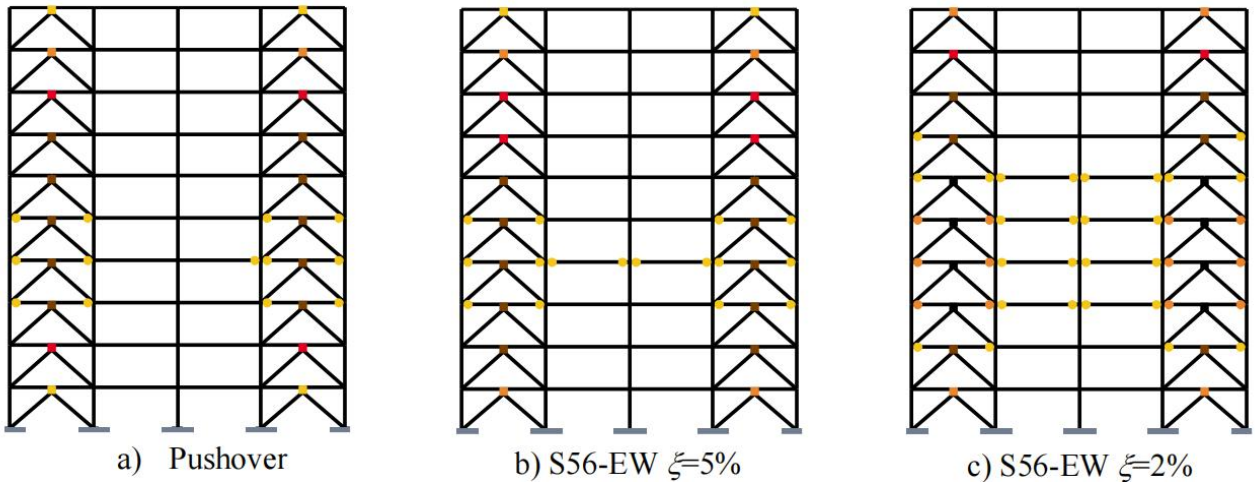

Figure 13. Comparative inelastic fluences mappings for model m10α75β25-2 ($\theta=45^0$, $k_2/k_{DDE}=0.03$).

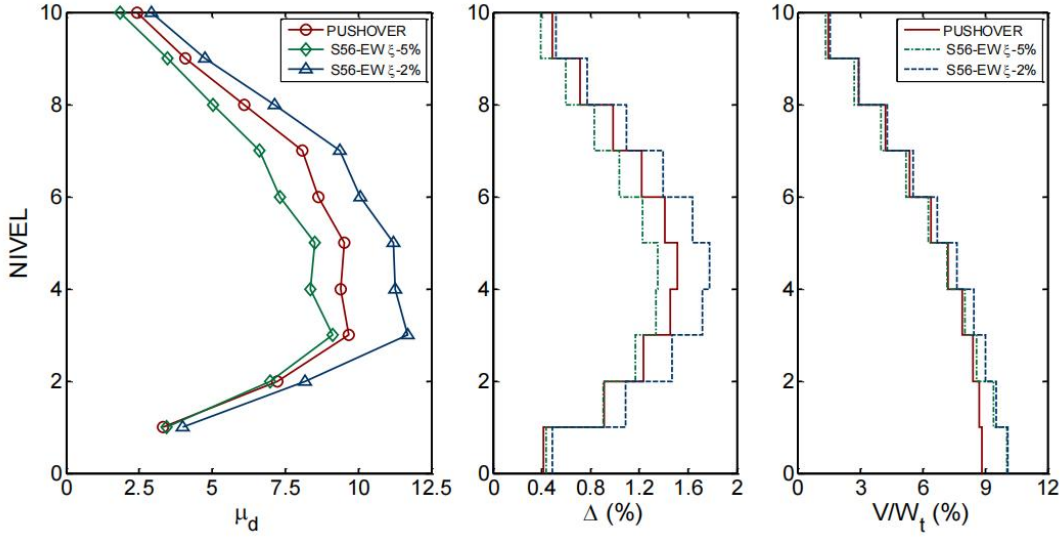

Figure 14. Comparative ductility demands μ_d of energy dissipaters, maximum interstory distortions and maximum interstory shear forces, for model m10α75β25-2 ($\theta=45^0$, $k_2/k_{DDE}=0.03$).

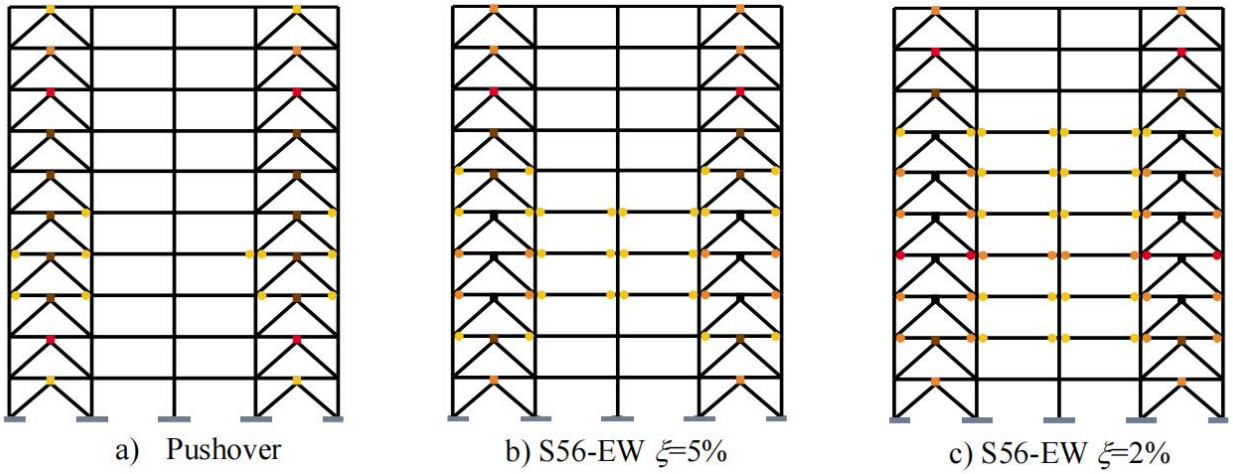

Figure 15. Comparison of inelastic fluences mappings for model m10α75β25-3 ($\theta=45^0$, $k_2/k_{DDE}=0.05$).

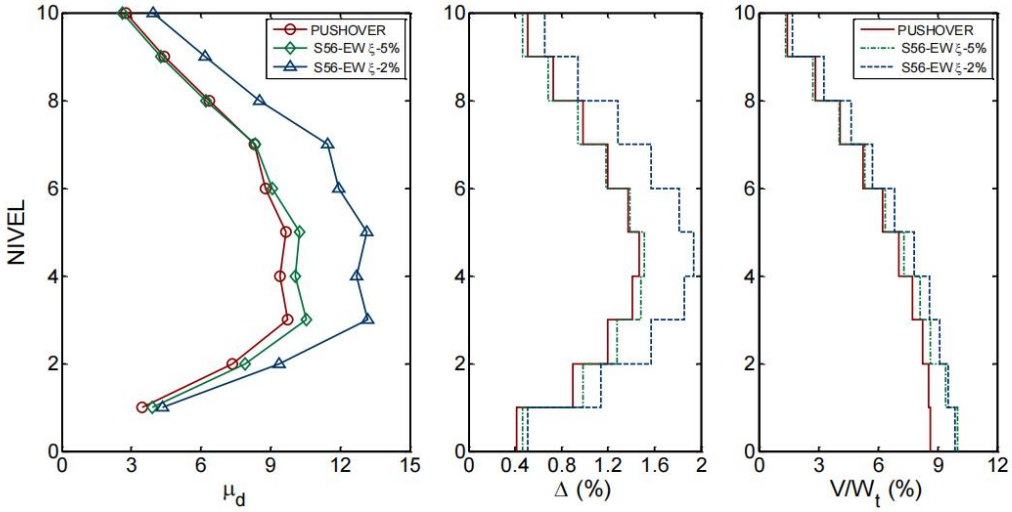

Figure 16. Comparative ductility demands μ_d of energy dissipaters, maximum interstory distortions and maximum shear forces in interstories, for model m10α75β25-3 ($\theta=45^0$, $k_2/k_{DDE}=0.05$).

When the nonlinear dynamic analyses are performed before the action of the S56-EW acceleration register and assuming an equivalent viscous damping $\xi=5\%$, congruent with what was assumed in the design, it can be seen that for the elastoplastic case (Figure 11b), the fluences mapping is very similar and, in fact, more resilient than that of the pushover analysis (Figure 11a), which is confirmed in Figure 12, where the curves obtained with the pushover analysis at the target ductility of the critical dissipators enclose the maximum responses obtained from the nonlinear dynamic analysis.

When the design is done assuming $k_2/k_{DDE}=0.03$ for the heatsinks, the flux mapping before the S56-EW log (Figure 13b) is similar to that of the pushover analysis (Figure 13a), but with a few more beam end fluences (three in total) in the expected (most demanded) zone. Again, Figure 14 shows that the curves obtained from the pushover analysis envelop those obtained considering $\xi=5\%$, completely in terms of maximum ductilities developed by the dissipators and maximum interstory distortions, and almost entirely for shear. It can be seen that precisely from the fourth floor onwards, the curve for $\xi=5\%$ leads to higher shears than that obtained with the pushover analysis, and this explains why there are additional influences on three beam ends in that interstory (Figure 13b).

When $k_2/k_{DDE}=0.05$ is considered in the design for the dissipators, the flux mapping at log S56-EW (Figure 15b) is still similar to that of the pushover analysis (Figure 15a), but with more beam fluences in the expected zone, as a function of the ductility demands of the dissipators. This happens because, as shown in Figure 16, the curves obtained from the

nonlinear dynamic analysis for ξ=5% slightly exceed those of the pushover analysis in terms of interstory distortions, and slightly more so in terms of the ductilities developed by the heatsinks. Therefore, by responding with a non-zero post-creep slope, this leads to higher interstory shear forces being demanded, which favors more beams to flow at the most demanded levels (levels 3, 4, and 5, as shown in Figure 15b).

The nonlinear dynamic analyses under the action of the S56-EW acceleration record indicate a scenario in which the design actions are exceeded, due to either: firstly, the design assumed an equivalent viscous damping higher than the most representative of the system considered, as allowed by the regulations (ξ=5% considered for all structural systems); or secondly, the extreme action exceeded the design spectrum. Thus, it is within expectations that, for the models designed considering that the heatsinks have a non-zero post-creep slope, the maximum dynamic responses exceed those obtained in the pushover analysis, both for k_2/k_{DDE}=0.03 (Figure 14) and for k_2/k_{DDE}=0.05 (Figure 16). However, for the perfect elastoplastic case (Figure 12), the pushover analysis curves continued to envelop those obtained for ξ=2%, partially due to the design process leading to a slightly stiffer structure (T=1.30s, Table 3) than those obtained when considering $k_2/k_{DDE}\neq 0$, resulting in lower demands for this model. The creep mappings obtained for ξ=2% (Figures 11c, 13c and 15c) are congruent with the proposed capacity design methodology, because if the extreme action exceeds the considered design resistance, the next line of inelastic defense after the energy dissipaters, which are designed to be the structural fuses, consists of the frame beams, with their creep being incipient and, at most, moderate. It should also be noted that when the design target ductility of the energy dissipaters is exceeded, more creep and greater magnitude (greater damage) should be expected in the frames as the post-creep slope of the energy dissipaters (k_2/k_{DDE}) increases, as a consequence that they would be transmitting greater shear forces to the frame as they continue to increase their ductility than those that were considered in their design.

4.3.3 15-level models

Figures 17 to 20 present the results of two models that were designed with the same stiffness balances, α=0.75 and β=0.25, and post-creep slopes of the dissipators, k_2/k_{DDE}=0.05. However, the cross-sections of the frame resisting elements vary significantly due to the different interstory heights and, therefore, the angle of inclination of the wind bracing with respect to the horizontal plane, θ. As can be seen in Table 3, this results in the fundamental periods of vibration being quite different, with the slenderest frame ($\theta=45^0$) having a greater period. Both models are in the rising branch of the spectrum where, utilizing a ductile design, a resonant dynamic response should be expected, as can be demonstrated with a ductility demand spectrum that takes into account the characteristics of these systems. In the nonlinear range, the critical period to obtain resonant responses is lower than the elastic fundamental period that defines the resonance, and it moves further away from the elastic fundamental period as the lateral yield strength decreases, and also depends on whether the system is ductile or degrades in stiffness and strength, as has been illustrated in previous works (Tena 1997 and 1998b, Tena-Colunga 2001) and is illustrated below.

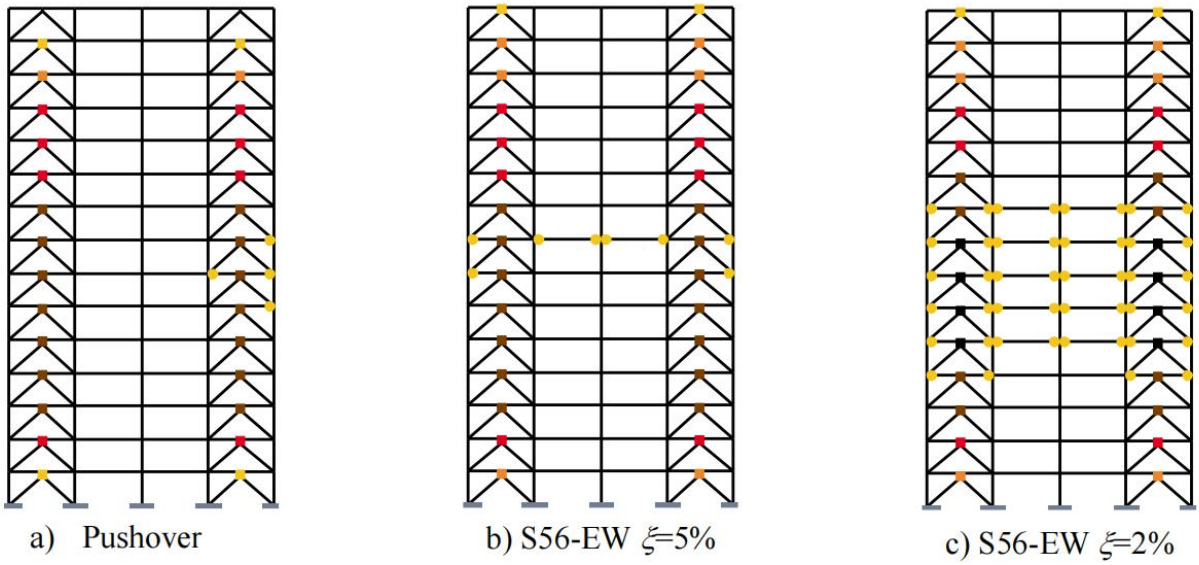

Figure 17. Comparative inelastic fluences mappings for the m15α75β25-1 model ($\theta=45^0$, $k_2/k_{DDE}=0.05$).

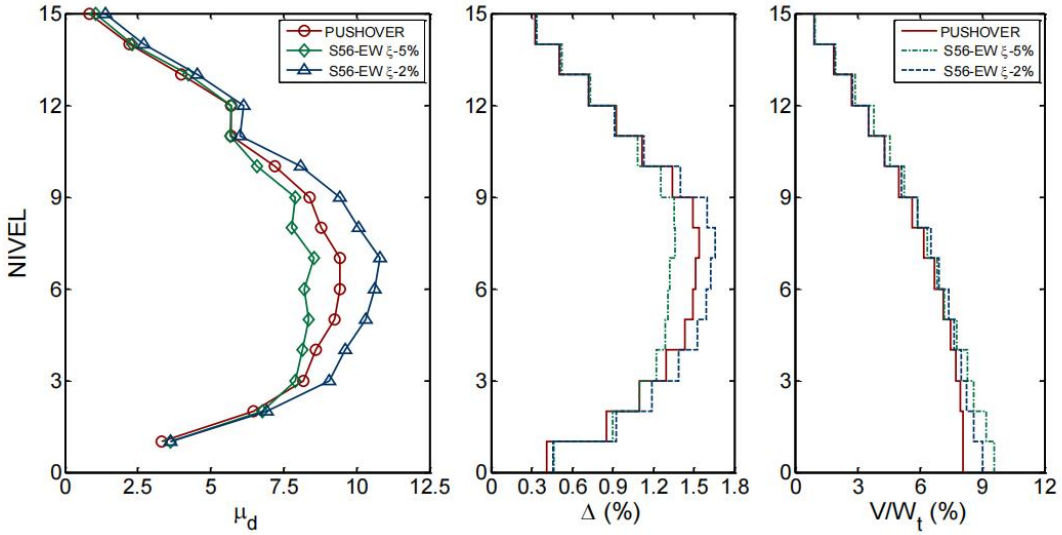

Figure 18. Comparative ductility demands μ_d of energy dissipaters, maximum interstory distortions and maximum shear forces in interstories, for model m15α75β25-1 ($\theta=45^0$, $k_2/k_{DDE}=0.05$).

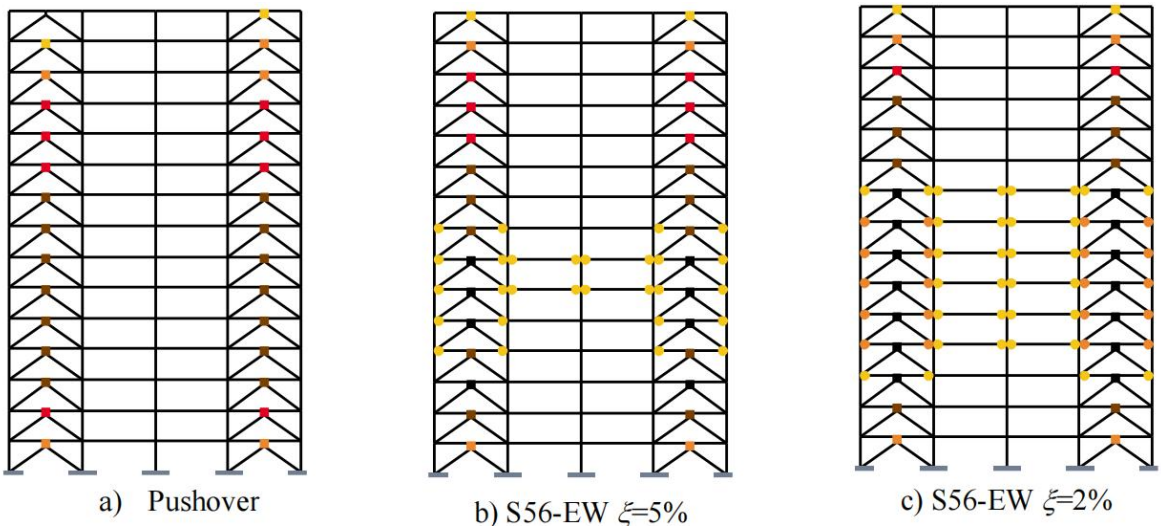

Figure 19. Comparison of inelastic fluences mappings for the m15α75β25-2 model ($\theta=40^0$, $k_2/k_{DDE}=0.05$).

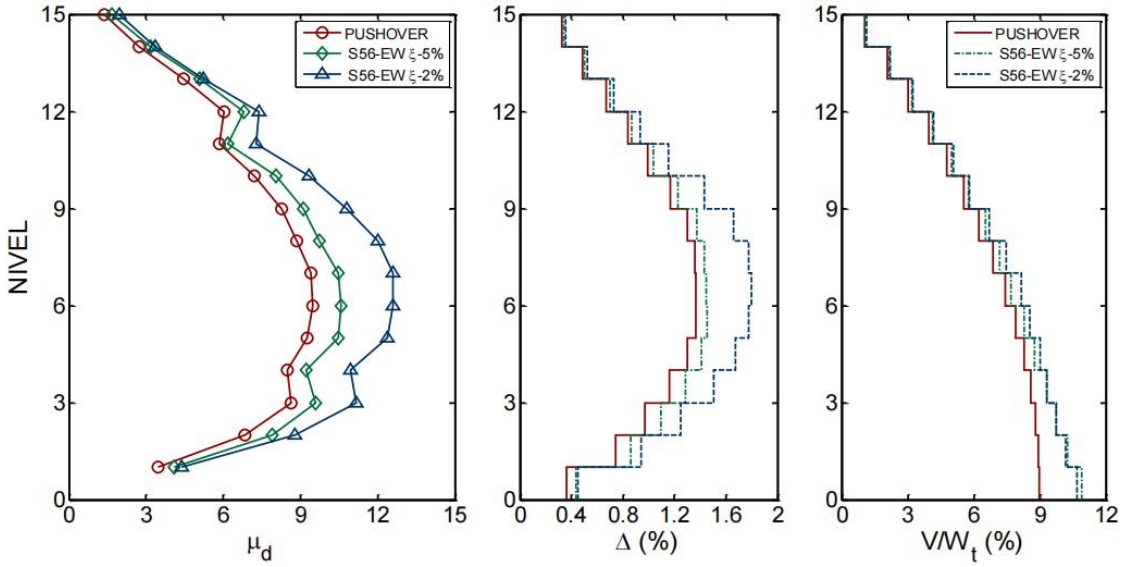

Figure 20. Comparison of ductility demands μ_d of energy dissipaters, maximum interstory distortions and maximum shear forces in the interstories, for model m15α75β25-2 ($\theta=40^0$, $k_2/k_{DDE}=0.05$).

According to the pushover analyses of each model, if taken to the target ductility μ_d of the critical dissipators, incipient creep is expected in some beams for the more flexible model ($\theta=45^0$, Figure 17a) and a 100% resilient design for $\theta=40^0$ (Figure 19a).

When the nonlinear dynamic analyses are performed under the action of the S56-EW acceleration record and assuming an equivalent viscous damping $\xi=5\%$, it can be seen that for the most flexible model ($\theta=45^0$), a response within the expected in terms of magnitude and location of the fluences (Figure 17b) is presented with respect to the results obtained from the pushover analysis. The above is confirmed in the maximum response curves of the maximum dissipator ductilities and maximum interstory distortions, which are practically enveloped by those obtained in the pushover analysis, except for the first two levels (Figure 18). The slight difference in the beam fluences is due to the dynamic excitation alternating directions (there is creep in beams on both sides) and to the slightly higher maximum interstory shears (Figure 18), in addition to a slight multi-modal participation.

For the slightly stiffer model ($\theta=40^0$), there is incipient creep in several beams (Figure 19b), still within tolerable limits, considering that the ductility demands of the dissipators exceeded those assumed in their design (Figure 20), so that higher distortions and shears developed (Figure 20). This is due to the frankly resonant response of the system, as illustrated and discussed below using the concept of ductility demand spectra (Tena 1997 and 1998b, Tena-Colunga 2001).

To better explain why for the stiffer model (m15α75β25-2, $\theta=40^0$, T=1.547s), comparatively higher demands were obtained than for the more flexible model (m15α75β25-1, $\theta=45^0$, T=1.842s), we will rely on the results shown in Figure 21. Using exclusively concepts of elastic structural dynamics, and based exclusively on the elastic response spectrum for $\xi=5\%$, it should be expected that the m15α75β25-2 model ($\theta=40^0$), whose elastic response for its fundamental period of vibration is indicated by a blue box in Figure 21, being further away from the resonant period of the elastic spectrum than model m15α75β25-1 ($\theta=45^0$), whose elastic response is indicated by a red circle, should also have a more favorable response in the nonlinear behavioral range (i.e., comparatively lower inelasticity).

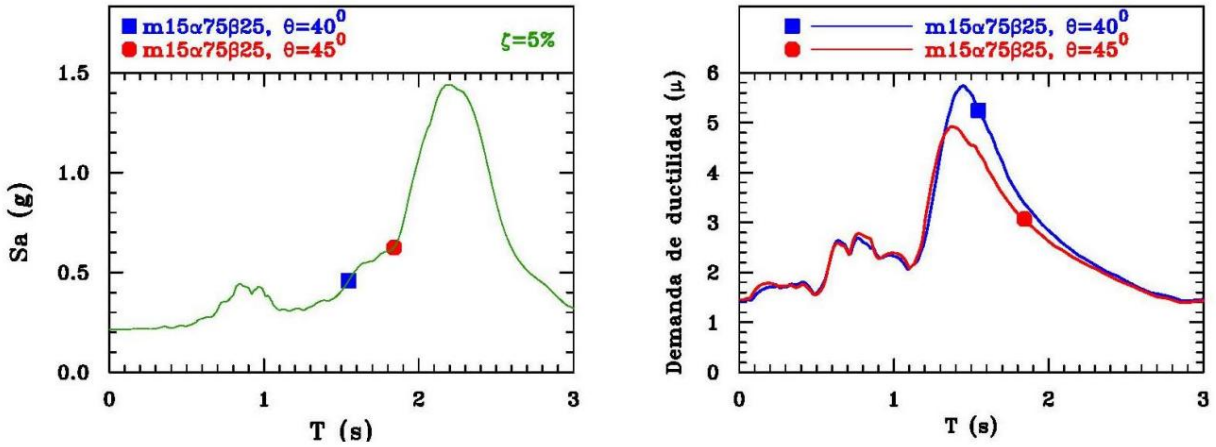

Figure 21. Elastic response and ductility demand spectra for the m15α75β25 models for the S56-EW acceleration record.

This is not necessarily true in highly nonlinear systems, since the ductility demands developed by the systems depend, among many other parameters, on their creep strength, the type of hysteretic behavior (bilinear with stiffening, elastoplastic, degrading in stiffness, degrading in strength, etc.), as discussed in previous works (Tena 1997 and 1998b, Tena-Colunga 2001). Therefore, ductility demand spectra were calculated for these two models, based on the global primary curves defined from the pushover analysis. Thus, the resulting bilinear curves had the following parameters that define the global bilinear model: a) for the m15α75β25-1 model ($\theta=45^0$), the normalized creep resistance was $V_y/W_t=0.195$ and the normalized post-creep slope with respect to elastic stiffness was $K_2/K_e=0.24$, b) for the 15α75β25-2 model ($\beta=40^0$), the global parameters were $V_y/W_t=0.191$ and $K_2/K_e=0.30$. Using these global parameters, the spectra of ductility demands were plotted, which are also shown in Figure 21, and in them it can be seen that, for the initial elastic period of the models, indeed, the maximum ductility demand of the initially stiffer system (model m15α75β25-2, $\theta=40^0$, indicated with a blue box that $\mu=5.24$ for T=1.547s), are higher than for the initially more flexible model (model m15α75β25-1, $\theta=45^0$, indicated with a red box that $\mu=3.07$ for T=1.842s). From the ductility demand spectra it is also seen that, for the considered normalized yield strengths (19.1% and 19.5% of the total weight of the structure), and for the post-creep slopes considered (24% and 30% of elastic), the frankly resonant responses in inelastic systems of these characteristics occur when the fundamental elastic periods of the systems are T=1.37s (model m15α75 β 25-1, $\theta=45^0$) and T=1.45s (model m15α75β25-2, $\theta=40^0$).

The authors consider it very important to illustrate this aspect, because for nonlinear systems, the resonant responses occur for elastic fundamental periods lower than the period associated with the elastic resonance, and tend to move further away from it as the normalized creep resistance is reduced, when the rest of the characteristics defining the hysteretic model remain unchanged. That is why abusing the reduction of design forces by ductility, considering very large ductilities, without taking into account how it affects the dynamic response of the structural system under study, is a very dangerous practice in the seismic-resistant design of structures, which can lead many structures to undesirable responses, even to an unforeseen collapse.

Figures 22 and 23 present the results of a model where, according to the pushover analysis, a fully resilient response is expected when the stiffness balances are $\alpha=0.5$ and $\beta=0.5$ and the post-creep slope of the dissipators is $k_2/k_{DDE}=0.03$ when $\theta=40^0$ (Figure 22a). When the nonlinear dynamic analyses are performed before the action of the S56-EW acceleration register and assuming an equivalent viscous damping $\xi=5\%$, there is full agreement in the fluences mapping for this system (Figure 22b), which has an elastic fundamental period T=1.55s (Table 3). Similarly, its maximum ductility and distortion responses are well enveloped by the pushover analysis (Figure 23).

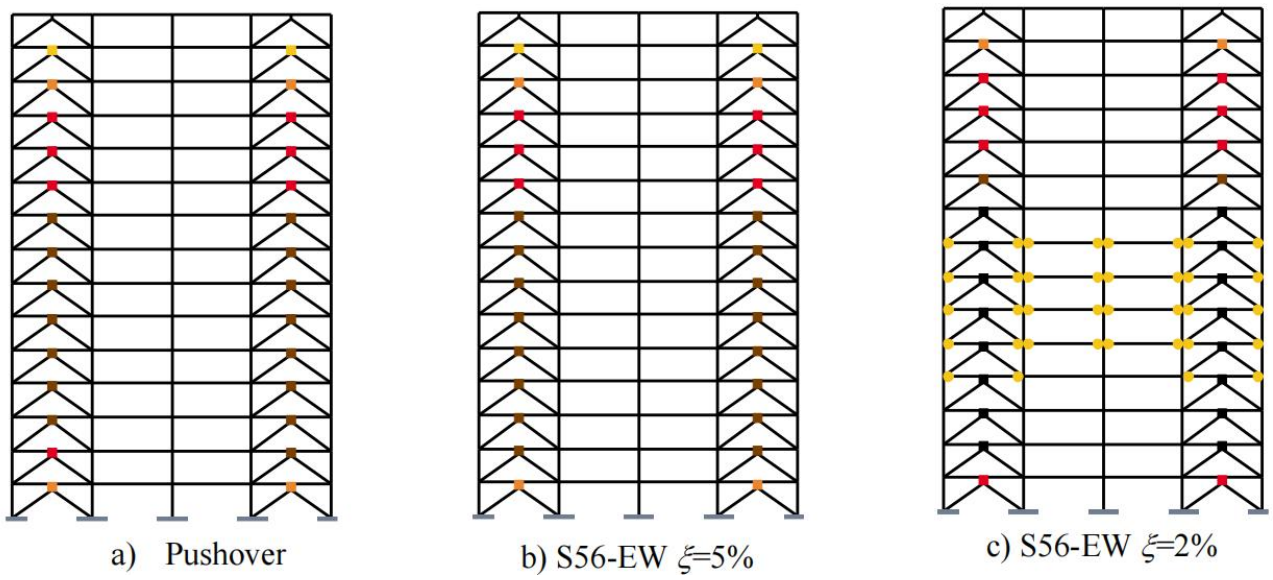

Figure 22. Comparison of inelastic fluences mappings for the m15α50β50 model ($\theta=40^0$, $k_2/k_{DDE}=0.03$).

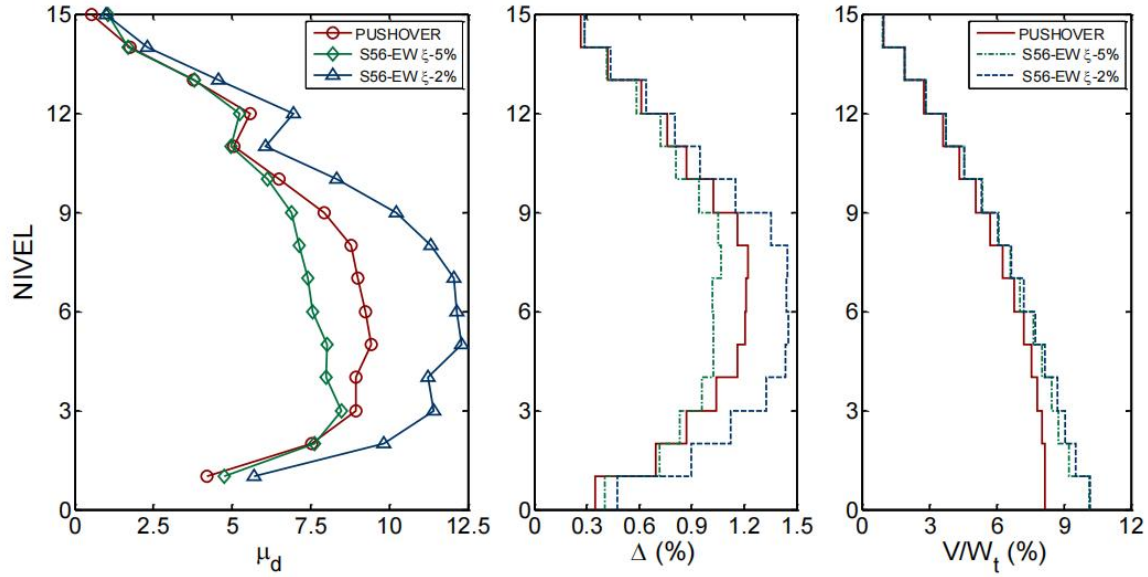

Figure 23. Comparison of ductility demands μ_d of the energy dissipaters, maximum interstory distortions and maximum shear forces in the interstories, for the m15α50β50 model ($\theta=40^0$, $k_2/k_{DDE}=0.03$).

Finally, for all the 15-level models studied (whether in resonance or not), when an equivalent viscous damping $\xi=2\%$ is considered, as expected, the maximum demands exceed those considered in their design (Figures 18, 20 and 23). However, it is again demonstrated that the proposed design process is robust, since these additional demands are taken by the second line of inelastic defense, which are the beams, most of which develop low creep (Figures 17c, 19c and 22c).

One thing that is strikingly notable about the models at resonance is that, in several mezzanines, the maximum shear envelopes of the system in the analyses for $\xi=5\%$ were higher than for $\xi=2\%$ (e.g., Figures 18 and 20), which may seem a priori unreasonable.. However, the reason for this is explained in detail below, in the discussion of the results of the 20-level models, where larger differences were observed and, therefore, it is easier to illustrate.

4.3.4 20-level models

Figures 24 to 29 present the results of two models that were also designed with the same stiffness balances, $\alpha=0.50$, $\beta=0.75$ and post-creep slopes of the dissipators $k_2/k_{DDE}=0.05$, where again the beam, column and wind girder sections vary

quite a bit as a result that the interstory heights and the wind girder inclination angles (θ) are different. From Table 3 we can see the impact on the fundamental periods of vibration, which are very different, T=2.162s when $\theta=45^0$ and T=1.773s when $\theta=40^0$. Again, if elastic structural dynamics criteria were used exclusively, both models would be on the rising branch of the spectrum in frank resonance (Figure 21), but their incursion into the nonlinear interval surely leads these models to lower dynamic responses, especially the higher period one, if one employs the concept of ductility demand spectrum (Figure 21).

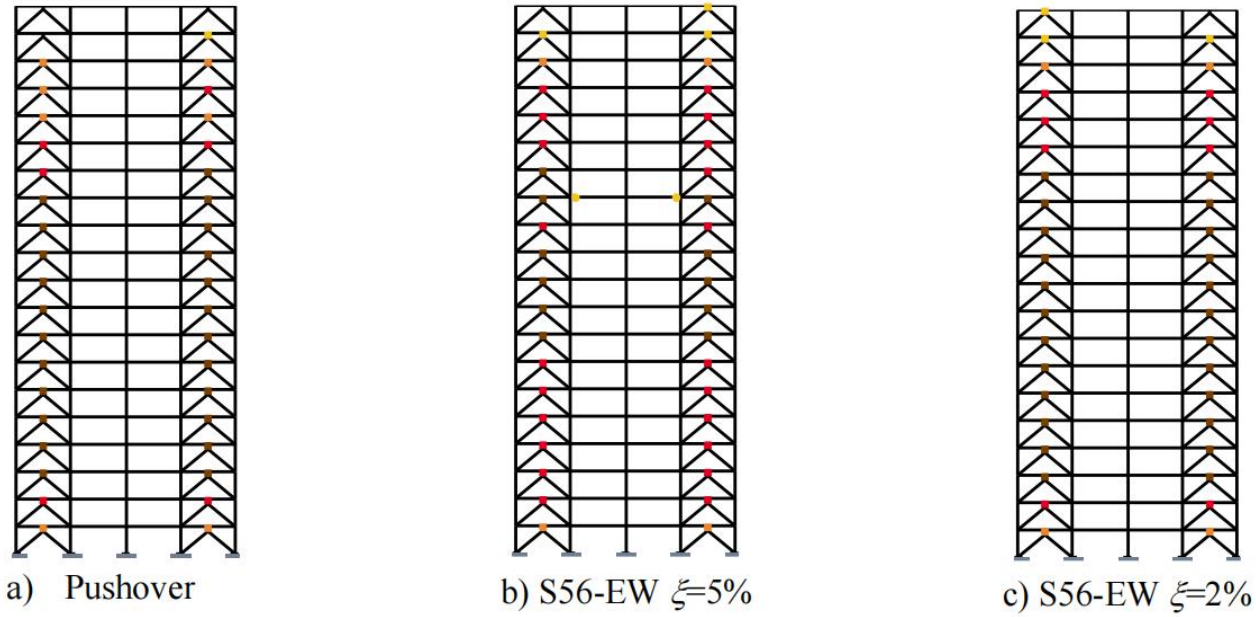

Figure 24. Comparative inelastic fluences mappings for model m20α50β75-1 ($\theta=45^0$, $k_2/k_{DDE}=0.05$).

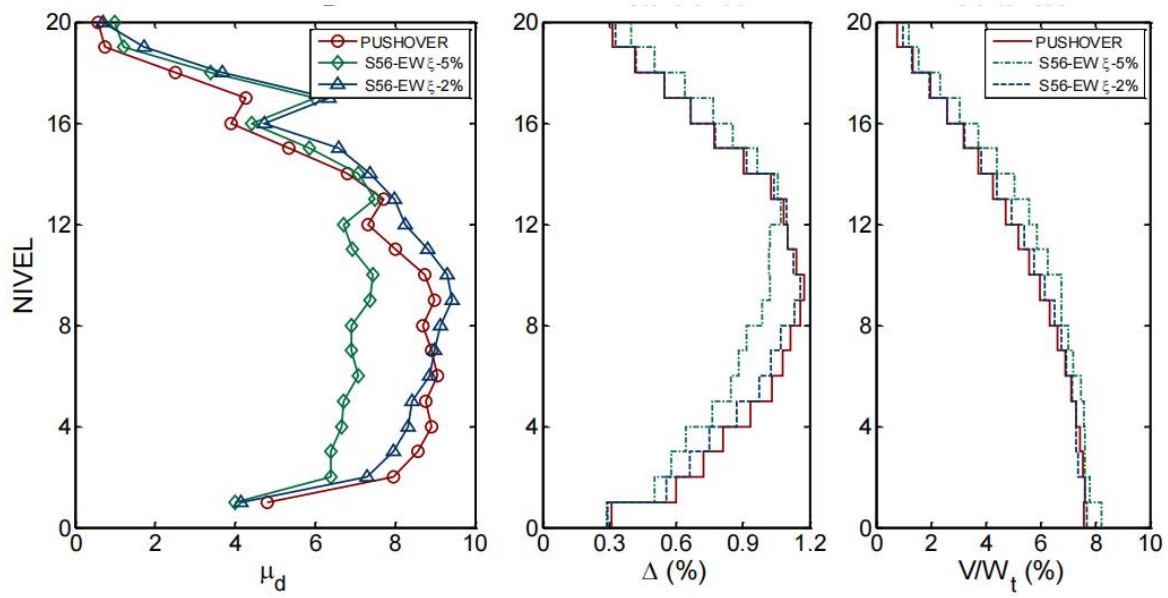

Figure 25. Comparative ductility demands μ_d of energy dissipaters, maximum interstory distortions and maximum shear forces in interstories, for model m20α50β75-1 ($\theta=45^0$, $k_2/k_{DDE}=0.05$).

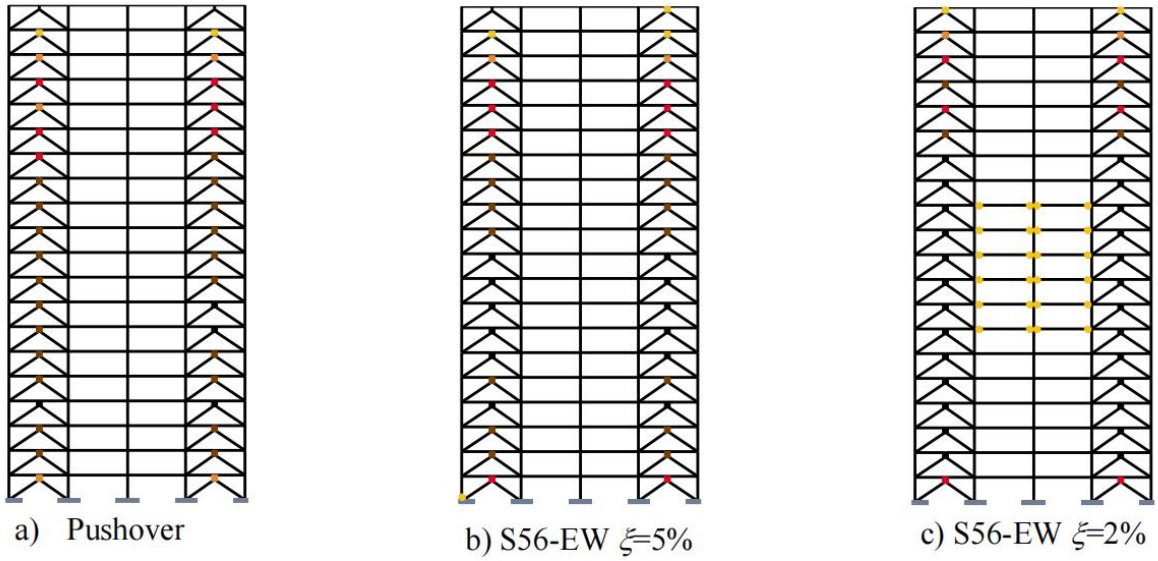

Figure 26. Comparative inelastic fluences mappings for model m20α50β75-2 ($\theta=40^0$, $k_2/k_{DDE}=0.05$).

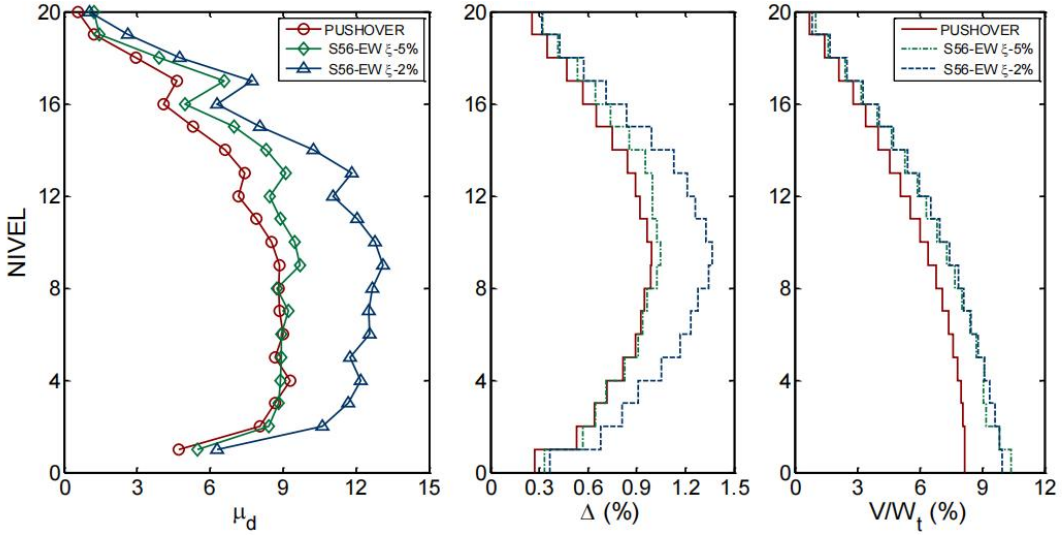

Figure 27. Comparative ductility demands μ_d of energy dissipaters, maximum interstory distortions and maximum shear forces in interstories, for model m20α50β75-2 ($\theta=40^0$, $k_2/k_{DDE}=0.05$).

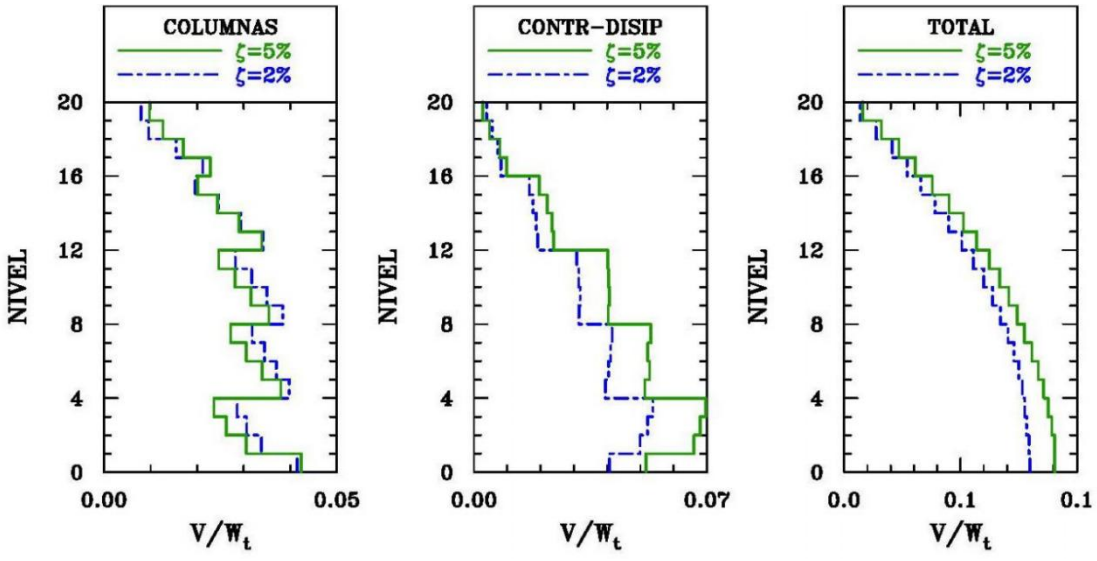

Figure 28. Comparison of maximum shear forces in mezzanine floors for model m20α50β75-1 ($\theta=45^0$, $k_2/k_{DDE}=0.05$).

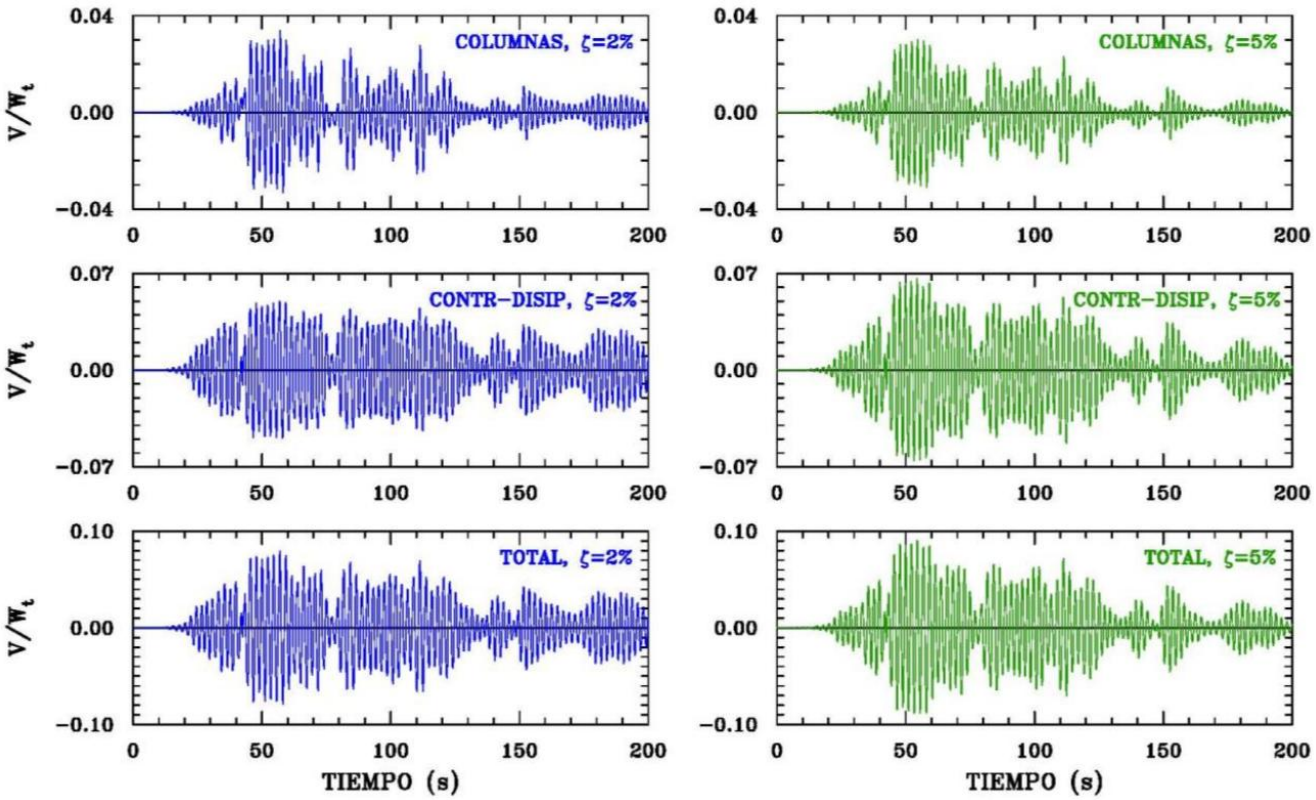

Figure 29. Comparative time histories of shear forces in interstory for model m20α50β75-1 ($\theta=45^0$, $k_2/k_{DDE}=0.05$).

According to the pushover analyses for each model, if the target ductility μd=10 of the critical heatsinks is taken, a 100% resilient design is expected in both cases (Figures 24a and 26a). When performing the nonlinear dynamic analyses under the action of the S56-EW acceleration register and assuming an equivalent viscous damping ξ=5%, it can be seen that for the more flexible model ($\theta=45^0$, Figure 24b) an almost 100% resilient response is presented, except for the incipient creep of two beams in mezzanine 13. For the stiffer model ($\theta=40^0$, Figure 26b), the response is 100% resilient.

From the maximum response curves of the maximum dissipater ductilities and maximum interstory distortions, it is observed that when $\theta=45^0$ (Figure 25), the pushover analysis curves completely envelop the curves for ξ=5% in the first 13 levels, but are exceeded starting at level 14, while when $\theta=40^0$ (Figure 27), the pushover analysis curves are exceeded starting at level 9. This is due to the fact that for buildings of these heights and characteristics, the impact of the higher modes of vibration on the dynamic response begins to be more important than for the heights previously studied.

Finally, in this case it can be seen that when considering ξ=2%, the maximum envelope demands slightly exceed those obtained with the pushover analysis for the more flexible model ($\theta=45^0$, Figure 25) and, notwithstanding, this, the flux mapping is still 100% resilient (Figure 24c). The demands significantly exceed those of the pushover analysis for the stiffer model ($\theta=40^0$, Figure 27); however, the resistant mechanism is still remarkably resilient, as only some incipient creep is present in the intermediate level beams (Figure 26c).

As can be seen in Figures 25 and 27, it is striking that, in these models, the maximum shear envelopes of the system in the analyses for ξ=5% resulted higher than for ξ=2%, especially for the model with $\theta=45^0$, where the largest differences are observed. In order to better understand why this happens, when common sense would indicate, based solely on knowledge of the dynamics of one degree of freedom systems, that the maximum responses should always be had for the system with the lowest equivalent viscous damping (in this case, ξ=2%), we proceeded to break down the maximum responses of this more complex system in more detail.

Thus, Figure 28 shows the distribution of the maximum dynamic shear resisted by: a) all the columns of the intermediate floor ("columns"), b) all the wind dissipators of the intermediate floor ("contr-disip"), and c) the complete system ("total"). In this figure, it can be seen that although higher maximum dynamic shears are developed for the complete system (total) when ξ=5%, this is mainly due to the fact that they come from the wind-dissipater system, where they are significantly higher for ξ=5% than for ξ=2% from level 1 to 18. However, in the columns, in almost all floors, the maximum floor shear is higher for ξ=2% than for ξ=5%.

As this explanation focusing solely on maximum responses might still seem insufficient, the time histories of the shears for each interstory were analyzed. For illustrative purposes, those of interstory 2 are presented in Figure 29, since it is a critical interstory where maximum responses in the columns are appreciable when ξ=2%, with sufficient difference. On the other hand, maximum responses in the interstory for the wind-dissipater system when ξ=5% are shown in Figure 28. From the observation of the shear time histories, an elementary principle of structural dynamics is verified: when the intensity of the seismic excitation decreases, the response of a system with higher equivalent viscous damping (in this case, ξ=5%) tends to attenuate or decrease in a more rapid and noticeable manner than that same system with lower equivalent viscous damping (in this case, ξ=2%). The above is fully complied with for the interstory shear histories of the columns, wind-damper system and of the complete system, mainly after 160 seconds of excitation (Figure 29), which is when the S56-EW record notably reduces its intensity (Figure 6). Then, although apriori it does not seem reasonable, and as also illustrated in Figure 29, it is possible to obtain higher responses in a complex nonlinear system of several degrees of freedom during the intense phase of the record for a higher equivalent viscous damping (ξ=5%) than for a lower one (ξ=2%).

4.3.5 25-level models

Figures 30 to 33 present the results of two 25-level models, model m25α75β25, with parameters α=0.75, β=0.25, $\theta=45^0$ and k_2/k_{DDE}=0. 03, in which it was obtained in the pushover analysis that a significant number of incipient fluences develop in beams at intermediate levels when the target ductility μ_d=10 is reached at critical dissipators (Figure 30a), and the m25α75β75 model, with parameters α=75, β=0.75,$\theta=40^0$ and k_2/k_{DDE}=0.03, in which pushover analysis yields a fully resilient mechanism at the target ductility μ_d=10 at the critical dissipators (Figure 32a).

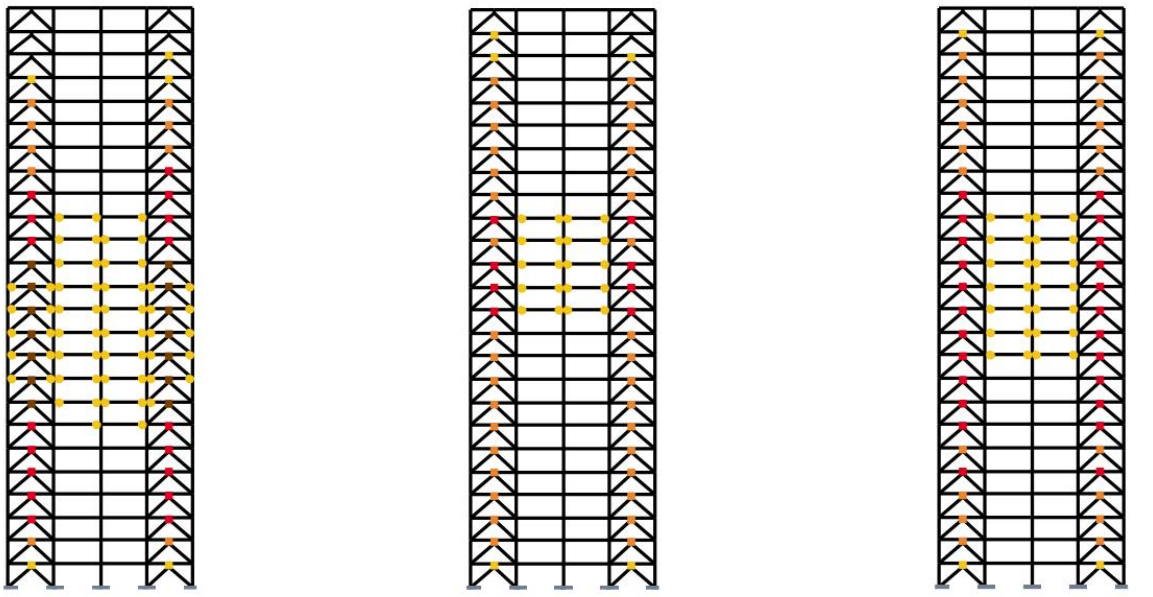

Figure 30. Comparison of inelastic fluences mappings for the m25α75β25 model ($\theta=45^0$, k_2/k_{DDE}=0.03).

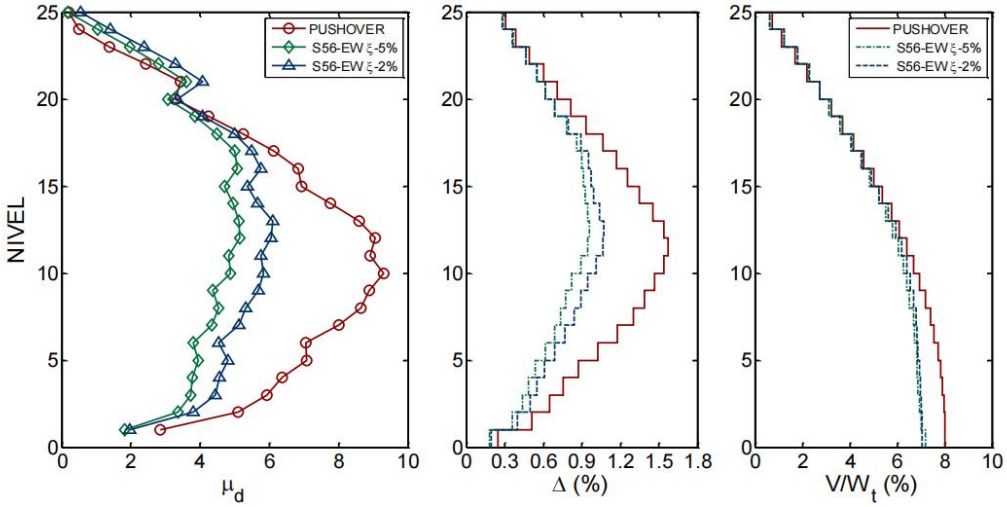

Figure 31. Comparative ductility demands μ_d of energy dissipaters, maximum interstory distortions and maximum shear forces in interstories, for model m25α75β25 ($\theta=45^0$, $k_2/k_{DDE}=0.03$).

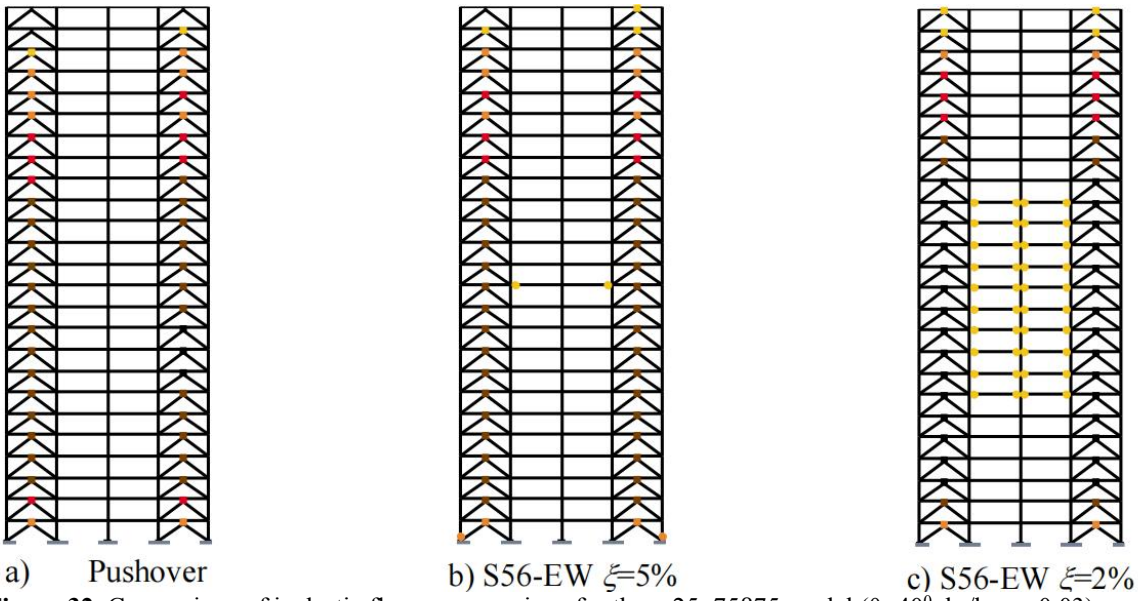

Figure 32. Comparison of inelastic fluences mappings for the m25α75β75 model ($\theta=40^0$, $k_2/k_{DDE}=0.03$).

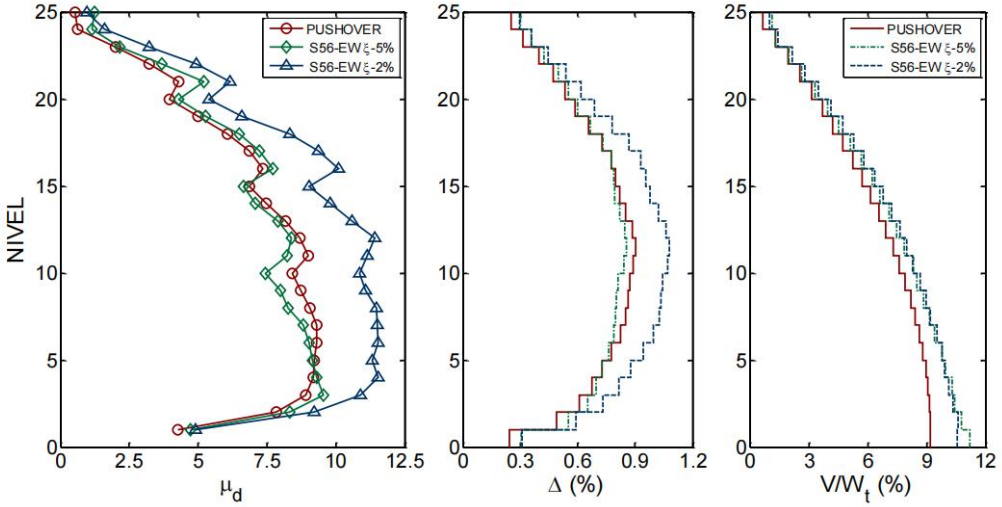

Figure 33. Comparative ductility demands μ_d of energy dissipaters, maximum interstory distortions and maximum shear forces in interstories, for model m25α75β75 ($\theta=40^0$, $k_2/k_{DDE}=0.03$).

For the first model (m25α75β25), the fundamental period of vibration is T=2.295s, which is close, but lies in the descending branch of the elastic resonance for the record under consideration (Figures 6 and 21). Therefore, in the nonlinear dynamic analyses before the S56-EW record, the maximum responses for ξ=5% and even for ξ=2% are perfectly enveloped by those obtained in the pushover analysis, except for the ductility demands of the dissipators between levels 21 and 25, due to the impact of the higher modes (Figure 31). Therefore, the developed fluences mappings are of lower intensity (Figures 30b and 30c) and are perfectly enveloped by the mapping obtained for the pushover analysis (Figure 30a).

For the second model (m25α75β75), the fundamental period of vibration is T=1.851s, and in this case the model is expected to enter the resonant response range (Figures 6 and 21), and then, in the nonlinear interval, to respond in a slightly lower demand range. Despite this, the creep mapping for ξ=5% (Figure 32b) agrees very well with that of the pushover analysis (Figure 32a), as only incipient creep develops in two beams, plus creep of two PB columns at their base, which is within what is tolerable in a resilient design in the face of extreme action. The maximum response curves of ductility demands and interstory distortions are very close and generally well enveloped by those of the pushover analysis; they only exceed them slightly at levels 1 to 3 and 16 to 25 (Figure 33). The maximum interstory shear forces are 10% to 20% higher than those estimated by the pushover analysis (Figure 33), but it should also be remembered that these models were designed for a 10% lower basal shear and that the accelerogram considered exceeds the elastic design spectrum (Figure 6).

From the observation of the results obtained for ξ=2%, the robustness of the proposed design procedure is confirmed, since if the design assumptions are significantly exceeded (maximum target ductility demands of the dissipators, distortions and interstory shears, Figure 33), the second inelastic defense mechanism, which are the beams, is activated, but only incipient creep develops (Figure 32c).

5. Final Comments and Conclusions

This paper presented the results of the nonlinear dynamic analyses of twelve building models that were designed according to a methodology that employs the method of forces and principles of design by capacity and structural fuse, which allows obtaining resilient seismic designs of structures based on ductile structural steel counterbuckled frames with hysteretic energy dissipaters.

The robustness of the proposed capacity and resilient design procedure is verified through a comparison of the response obtained for 12 critical models using nonlinear stepwise dynamic analysis. Additionally, the validity of the global seismic design parameters (Q, R, Δ_y and Δ_u) and the initial (elastic) stiffness balances between the frame system and the total system (α), as well as between the dissipator and the supporting counterbuckling (β), are confirmed. These design elements and parameters were previously proposed and explained in detail in earlier works. The comparison is made relative to the response obtained through nonlinear static analysis under increasing monotonic load (pushover), which was used to define the resilient design mechanisms and global seismic design parameters.

It is confirmed and demonstrated that the resilient seismic design mechanisms obtained by pushover analysis are fulfilled for the vast majority of the 12 models studied. In this analysis, the energy dissipaters work inelastically, essentially serving as structural fuses. They allow only incipient (low intensity) creep to develop in a few beams. This fulfillment is observed in the face of an extreme design action that is compatible with the design assumptions of the models. The results obtained for the artificial record S56-EW for ξ=5% corroborate this, even in cases where the models respond dynamically in the resonant fringe. It is also verified that, if the dynamic excitation exceeds the resistance or demand parameters assumed during the design of the models, as demonstrated by the results obtained for the artificial record S56-EW with ξ=2%, the second line of defense within the system is activated. This involves the incipient creep of a very small number

of beams in the frame. It should be emphasized that even in cases where the structure responds in the resonant fringe, this creep remains limited to a few beams.

Based on the results presented, it is confirmed that it is very feasible to resiliently design structures based on ductile structural steel counterframes with hysteretic energy dissipaters, using the method of forces and principles of design by capacity and structural fuse. This includes tall and slender buildings (20 and 25-story models), where it should be noted that the response of the higher modes begins to be important in the response of the last levels. Therefore, the global seismic design parameters and optimal stiffness balances α and β derived from the pushover analyses can be used with confidence, as well as the values obtained for the global seismic design parameters Q, R, Δ_y and Δ_u.

Finally, the authors stress the importance of noting, as demonstrated in this study, that for nonlinear systems, resonant responses occur at elastic fundamental periods shorter than those associated with elastic resonance. These responses tend to shift further away from the elastic resonance period as the normalized creep resistance decreases, assuming the remaining hysteretic model characteristics remain constant. Consequently, excessive reduction of design forces through ductility considerations, particularly when very large ductilities are assumed without considering their impact on a structure's dynamic response, poses a significant risk in seismic-resistant design. This practice can lead to undesirable structural responses, including potential collapse, and is not limited to the specific structural system studied here. Rather, it is a general observation that has been previously demonstrated in other structural systems as well.

Acknowledgements

Héctor Hernández Ramírez is grateful for the scholarship granted by the Consejo Nacional de Ciencia y Tecnología de México (Conacyt), which allowed him to be involved in this research project in the development of his master's thesis in the Postgraduate Program of Structural Engineering at UAM Azcapotzalco. The authors thank Dr. Luis Eduardo Pérez Rocha for generating the synthetic accelerogram for station CO56 used in this study.

Conflicts of Interest

The author declares no conflicts of interest regarding the publication of this paper.

References

[1] Aguiar, R, L García, E Menéndez, M Zevallos y J Palacios (2016a), "Análisis y reforzamiento de una estructura afectada por el terremoto del 16 de abril de 2016", *Revista Ingeniosos*, Vol. 1, Art. 1, pp. 1-16, marzo-septiembre.

[2] Aguiar, R, M Rodríguez y D Mora (2016b), "Análisis sísmico de estructuras con disipadores de energía ADAS o TADAS", Monografía CIMNE IS-75, Centro Internacional de Métodos Numéricos en Ingeniería, Barcelona, España, ISBN: 978-84-945077-5-5.

[3] Benedetti, A, L Landi y D G Merenda (2014), "Displacement-based design of an energy dissipating system for seismic upgrading of existing masonry structures", *Journal of Earthquake Engineering*, Vol. 18, No. 4, pp. 477-501, DOI: 10.1080/13632469.2014.897274.

[4] Chen, Z Y, H Ge, A Kasai y T Usami (2007), "Simplified seismic design approach for steel portal frame piers with hysteretic dampers", *Earthquake Engineering and Structural Dynamics*, Vol. 36, No. 4, pp. 541-562. DOI: 10.1002/eqe.643

[5] Del Valle, E (1988), "Amortiguamiento adicional para reducir efectos sísmicos", *Revista de Ingeniería Sísmica*, No. 32, pp. 49-76.

[6] Foti, D, L M. Bozzo y F López-Almansa (1998), "Numerical efficiency assessment of energy dissipators for seismic protection of buildings", *Earthquake Engineering and Structural Dynamics*, Vol. 27, pp. 543-556. DOI: 10.1002/(SICI)1096-9845(199806)27:6<543::AID-EQE733>3.0.CO;2-9

[7] Hernández, H (2015), "Propuesta de diseño sísmico para marcos de acero con disipadores de energía histeréticos", Tesis de Maestría, Posgrado en Ingeniería Estructural, División de Ciencias Básicas e Ingeniería, Universidad Autónoma Metropolitana Azcapotzalco, julio.

[8] Nangullasmú, H J y A Tena (2016), "Requisitos mínimos de detallado dúctil en marcos de concreto reforzado protegidos con disipadores histeréticos de energía", *Revista de Ingeniería Sísmica*, No. 95, pp. 1-32, julio-diciembre, DOI: 10.18867/ris.95.381.

[9] NTCS-04 (2004), "Normas Técnicas Complementarias para Diseño por Sismo", Gaceta Oficial del Distrito Federal, Tomo II, No. 103-BIS, octubre.

[10] Ramírez, O M, M C Constantinou, C A Kircher, A S Whittaker, M W Johnson, J D Gómez y C Z Chryzostomou (2001), "Development and evaluation of simplified procedures for analysis and design of buildings with passive energy dissipation systems", Technical Report MCEER-00-0010, Multidisciplinary Center for Earthquake Engineering Research, State University of New York at Buffalo.

[11] Rosenblueth, E, M Ordaz, F J Sánchez-Sesma y S K Singh (1989), "The Mexico earthquake of September 19, 1985 - Design spectra for Mexico´s Federal District", *Earthquake Spectra,* Vol. 5, No. 1, pp. 273-291. DOI: 10.1193/1.1585523

[12] Scholl, R E (1993), "Fundamental design issues for supplemental damping applications", *Earthquake Spectra*, Vol. 9, No.3, pp. 627-636. DOI: 10.1193/1.1585732

[13] Symans, M D, F A Charney, A S Whittaker, M C Constantinou, C A Kircher, M W Johnson y R J McNamara (2008), "Energy dissipation systems for seismic applications: current practice and recent developments", *ASCE Journal of Structural Engineering*, Vol. 134, No. 1, pp. 3-21. DOI: 10.1061/(ASCE)0733-9445(2008)134:1(3)

[14] Tena, A (1997), "Espectros inelásticos de demandas de ductilidad para la evaluación de estructuras existentes ante sismos", Memorias, XI Congreso Nacional de Ingeniería Sísmica, Veracruz, Vol. I, pp. 671-682, noviembre.

[15] Tena, A (1998a), "Modelado analítico de edificios con disipadores de energía, aplicaciones en proyectos de reestructuración", Memorias, V Simposio Nacional de Ingeniería Sísmica: Disipadores de energía para controlar la respuesta sísmica de edificios, Toluca, Estado de México, pp. 85-120, septiembre.

[16] Tena, A (1998b), "Evaluación sísmica simplificada de estructuras existentes", *Revista de Ingeniería Sísmica*, No. 59, pp. 29-62, julio-diciembre, DOI: 10.18867/ris.59.251.

[17] Tena, A (2000), "Modelado analítico de edificios con disipadores de energía", *Revista de Ingeniería Sísmica*, No. 62, pp. 29-62, DOI: 10.18867/ris.62.253.

[18] Tena, A (2010), "A 25 años del sismo de septiembre de 1985: Breves reflexiones sobre los espectros de diseño sísmico", Memorias, XI Simposio Nacional de Ingeniería Sísmica, a 25 años del sismo de 1985: Aprendizaje, Conciencia y Prevención, México, DF, CDROM, pp. 1-9, septiembre.

[19] Tena, A y H J Nangullasmú (2013), "Diseño sísmico de marcos no dúctiles de concreto reforzado con disipadores de energía histeréticos. Definición de parámetros de diseño", *Revista Internacional de Desastres Naturales, Accidentes e Infraestructura Civil*, Vol. 13, No. 2, pp. 275-299.

[20] Tena, A, H J Nangullasmú, H Hernández y A Gama (2016), "Diseño sísmico conforme a reglamento de edificios estructurados con base en marcos contraventeados con disipadores de energía histeréticos", Memorias, XIV Simposio Nacional de Ingeniería Sísmica, León, Guanajuato, CDROM, pp. 1-57, junio-julio.

[21] Tena, A y H Hernández (2016), "Definición de parámetros globales de diseño sísmico de marcos dúctiles de acero con disipadores de energía histeréticos", *Revista Internacional de Desastres Naturales, Accidentes e Infraestructura*

Civil, Vol. 16, No. 1, pp. 19-47.

[22] Tena, A y H Hernández (2017), "Diseño sísmico resiliente de marcos dúctiles de acero con fusibles estructurales", *Revista Internacional de Ingeniería de Estructuras*, Vol. 22, No. 4, pp. 421-457.

[23] Tena, A y A Gama (2017), "Determinación de parámetros de diseño sísmico para marcos dúctiles de concreto reforzado con disipadores de energía histeréticos", *Revista Sul-americana de Engenharia Estrutural*, Vol. 14, No. 1, pp. 36-58, DOI: 10535/rsaee.v14i1.6496.

[24] Tena-Colunga, A y D Pérez-Moreno (1994), "Seismic upgrading of a nine-story building at Mexico City's lake-bed zone using U-Shaped energy dissipation devices", Memorias, 9th International Seminar on Earthquake Prognostics, San José, Costa Rica, septiembre, DOI:10.13140/2.1.1991.9684.

[25] Tena-Colunga, A, E Del Valle y D Pérez-Moreno (1996), "Issues on the seismic retrofit of a building near resonant response and structural pounding", *Earthquake Spectra*, Vol. 12, No. 3, pp. 567-597, DOI: 10.1193/1.1585897.

[26] Tena-Colunga, A y A Vergara (1997), "Comparative study on the seismic retrofit of a mid-rise steel building: steel bracing vs energy dissipation", *Earthquake Engineering & Structural Dynamics*, Vol. 26, No. 6, pp. 637-645, DOI: 10.1002/(SICI)1096-9845(199706)26:6<637::AID-EQE666>3.0.CO;2-R.

[27] Tena-Colunga, A (2001), "Displacement ductility demand spectra for the seismic evaluation of structures", *Engineering Structures*, Vol. 23, No. 10, pp. 1319-1330, DOI: 10.1016/S0141-0296(01)00025-6.

[28] Tena-Colunga, A (2007), "State of the art and state of the practice for energy dissipation and seismic isolation of structures in Mexico", Memorias, 10th World Conference on Seismic Isolation, Energy Dissipation and Active Vibration Control of Structures, Estambul, Turquía, CD-ROM, mayo.

[29] Tena-Colunga, A y H J Nangullasmú-Hernández (2015), "Assessment of seismic design parameters of moment resisting RC braced frames with metallic fuses", *Engineering Structures*, Vol. 95, pp. 138-153, DOI: 10.1016/j.engstruct.2015.03.062.

[30] Tena-Colunga, A y H Hernández-Ramírez (2017), "Code-oriented global design parameters for moment-resisting steel frames with metallic structural fuses", *Frontiers in Built Environment*, Vol. 3, Article 19, DOI: 10.3389/fbuil.2017.00019.

[31] Vargas, R y M Bruneau (2006), "Analytical investigation of the structural fuse concept", Technical Report MCEER-06-0004, Multidisciplinary Center for Earthquake Engineering Research, University at Buffalo, State University of New York, March.

[32] Vargas, R y M Bruneau (2009), "Analytical response and design of buildings with metallic structural fuses. I", *ASCE Journal of Structural Engineering,* Vol. 135, No. 4, pp. 386-393. DOI: 10.1061/(ASCE)0733-9445(2009)135:4(386)

[33] Wu, J y R E Hanson (1987), "Inelastic response of structures with high damping subjected to earthquakes", Report UMCE 87-9, Department of Civil Engineering, The University of Michigan, noviembre.